Chapter 5 Chemical Vapour Infiltration

5.1 Introduction

Chemical vapour infiltration (CVI) was initially proposed and developed by Bickerdike [1] in 1962 to increase the density of porous carbon. The earliest patent was to infiltrate the porous alumina preform with chromium carbide by Jenkins [2] in 1964. CVI was then described for the densification of C/C composites by Kotlensky in 1973 [3]. CVI techniques have been widely investigated since. In the early 1970s Professor Fitzer's group [4] at Karlsruhe University started to investigate SiC CVI for fibre-reinforced composites. Meanwhile, Professor Naslain's group [5] at Bordeaux University began the development of an isothermal isobaric CVI (I-CVI) technique to an fabricate carbon-fibre-reinforced silicon carbide composite aimed improving the oxidation resistance of C/C composites. In 1984 a forced CVI (F-CVI) technique was demonstrated by Professor Lackey's group [6] at Oak Ridge National Laboratory, USA. The commercialisation of the I-CVI technique for ceramic-matrix composites was first carried out at Societe Europeenne de Propulsion (SEP), France and at Du Pont, USA.

CVI technology is considered an extension of CVD technology. CVD is a process in which the coating is deposited on a completely dense solid surface at high temperatures from gaseous precursors. CVD has been successfully used to fabricate special coatings and thin-film electronic devices since the 1960s. CVI processes are special applications of CVD and the deposition takes place within porous preforms relying on a standard CVD reaction. This CVD coating penetrates and grows into the porous structure in a continuous layer-by-layer manner, forming the composite matrix. CVI, therefore, is a way of fabricating a new type of structural material which has many advantages. Similar to the CVD model, Fitzer [7] proposed a model for the CVI process as shown in Figure 5.1. The CVI process typically consists of the following steps:

1. gaseous precursors penetrate into the boundary layer from the bulk gas;
2. gaseous species are transported by diffusion into the pores within the fibre preform;
3. gaseous species are adsorbed onto the inner surface of the pore;
4. chemical reactions take place and coating forms on the fibre surface;
5. volatile by-products are desorbed from the surface;
6. gaseous by-products are transport outwards by diffusion; and
7. gaseous by-products return to the bulk gas through the boundary layer.

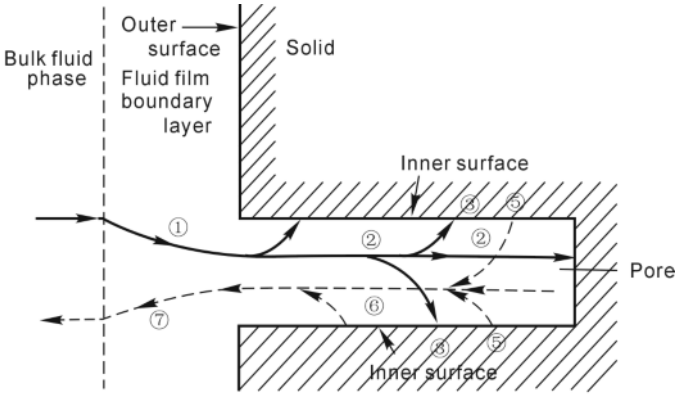

Figure 5.1. A CVI model [7]

Compared with conventional techniques for fabricating ceramic-matrix composites, such as hot pressing (HP), reactive melt infiltration (RMI) and polymer impregnation and pyrolysis (PIP), CVI techniques have distinct advantages, which can be summarised as follows [8, 9]:

5.1.1.1 Near-net-shape Process

During the densification process the preforms are usually placed in the reaction chamber at a reduced pressure. As there is no pressing or other mechanical forces exerted on the fibre preform during the densification process the final shape of the preform is very close to the desired shape and there is no large amount of material to be further removed by the machining method. The starting preforms therefore can be very complex in terms of shapes as this should represent the final finished target component.

5.1.1.2 Minimal Mechanical Damage to the Fibres

Damage to the fibres can easily happen if the component is exposed in an environment with high temperatures and mechanical loads. CVI processes normally take place at relatively low temperatures, typically in a range of 900 to 1100°C. This temperature is contrasted to high processing temperatures, usually above 2000°C when a traditional sintering method is employed to fabricate the high-temperature SiC-matrix material. Using the CVI technique, SiC material can be easily deposited at 1000°C via the following chemical reaction:

$$CH_3SiCl_{3(V)}+\text{excessive } H_2=SiC_{(s)}+3HCl+\text{excessive } H_2 \quad (5.1)$$

In such conditions the brittle ceramic fibres, such as Nicalon SiC and Al_2O_3 fibres, remain undamaged during the CVI process. However, conventional techniques for the fabrication of ceramic-matrix composites such as hot pressing take place at extremely high temperatures (2000°C) and under high mechanical stresses (30 MPa), which usually severely damage the fibres.

Moreover, the service temperature of CVI materials can be much higher than CVI processing temperatures. The reason for this advantageous feature is that the ceramic matrix produced by CVI is much purer than that obtained with the hot-pressing method, in which sintering additives are generally needed.

5.1.1.3 Variety of Ceramic-matrix Materials

Through many research and development studies CVI processes have already been established as good ways of fabricating a wide variety of ceramic-matrix materials including boride (e.g. SiB_2, SiB_6,TiB_2, ZrB_2), carbide (e.g. SiC, B_4C,HfC, TiC etc.), nitride (BN, Si_3N_4 etc.), oxide (Al_2O_3, ZrO_2 etc.) and silicide (e.g. $TiSi_2$, $MoSi_2$). Owing to their superior mechanical properties fibre-reinforced SiC and related matrix composites have been widely produced on an industrial scale, mainly for applications in the aeronautic and space fields. It is expected that the number of composite components produced by CVI techniques will increase and more materials will become available.

5.1.1.4 A Flexible Fabrication Technique for Smart and Delicate Microstructures

One of the outstanding advantages of CVI processes over other CVD approaches is its suitability to deposit nanometre-scale coatings (10^1~10^2 nm) as an interphase on the surface of individual fibres within a preform. This is expected to be of particular importance and interest in the fabrication of tough ceramic-matrix composites. The interface is the key to controlling the mode of crack propagation between the fibre and the matrix. According to recently developed theories of interface fracture, the path of a crack can be deflected along the interface, caused by the pull-out of the fibre, thereby increasing the required total work of fracture. The ability to deposit a multilayered matrix is used to produce self-healing ceramic-matrix composites which allow for a long service lifetime an oxidation atmosphere.

The main drawback of the CVI techniques is the long processing time of infiltration, normally in the range of a hundred hours. This is coupled with a very slow rate of deposition associated with a relatively low conversion efficiency of the precursor. To address this deficiency new manufacturing approaches have been explored to develop rapid infiltration techniques and so far most of these attempts remain as research work being investigated in laboratories. Another potential problem is that CVI composites exhibit some residual open porosity. This would be a drawback for applications where gas or liquid tightness is strictly required.

According to the controlling parameters used in the process, CVI approaches can be classified into five typical categories [9]: isothermal/isobaric CVI (I-CVI), forced-flow CVI (F-CVI), thermal gradient/isobaric CVI (TG-CVI), pulsed CVI (P-CVI) and liquid immersion CVI (LI-CVI). There are more than ten CVI techniques if a particular method is coupled with plasma, microwave or a catalyst to enhance the process [10]. Some representative techniques are discussed in this chapter as follows.

5.2 Isothermal and Isobaric Chemical Vapour Infiltration

5.2.1 General Description

Isothermal and isobaric CVI (I-CVI), a relatively easy and the oldest hot-wall technique, is still widely used in research and in industry. The key feature of this approach is that both temperature and pressure are kept constant during the infiltration process. Because of this its main advantage is good consistency of the finished product due to strict yet easy thermal and pressure parameter control. In particular a large number of complex preforms can be densified simultaneously, as shown in Figure 5.2.

For the infiltration of SiC methyltrichlorosilane (MTS with a molecular formula of CH_3SiCl_3) is employed as the precursor, which is carried using a hydrogen bubbling method. The normal processing conditions include a temperature of 1000°C, an H_2/MTS mol ratio of 10 with Ar often used as dilute gas. Usually the process is performed at a reduced pressure of 10 to 30 kPa. The reasons for using reduced pressures in I-CVI are (1) to enable higher gas-phase diffusivity, leading to more uniform distributions of density and microstructure within the composites, and (2) to reduce or eliminate undesirable gas nucleation and the formation of deleterious by-products, such as tar and soot in the case of carbon CVI. The temperature of the working zone is measured and controlled by a thermocouple and its driven actuator to control the heating elements of the system. The pressure is measured by a pressure gauge and controlled by a throttle valve on the vacuum system.

5.2.2 Isothermal and Isobaric Chemical Vapour Infiltration Process Model

For I-CVI processes, the driving force for mass transport is the concentration gradient of the reactant gaseous species as shown in Figure 5.3. During the densification process the precursor gases flow over the preforms at a reduced pressure. Then they diffuse into the porous and fibrous preforms, react and form a

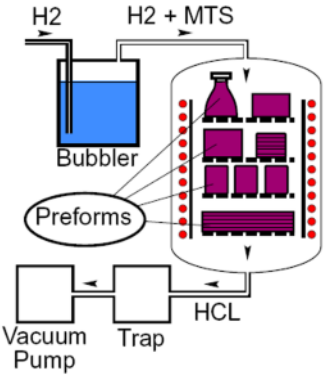

Figure 5.2. I-CVI schematic diagram of hot-wall infiltration chamber for SiC-matrix composites [11]

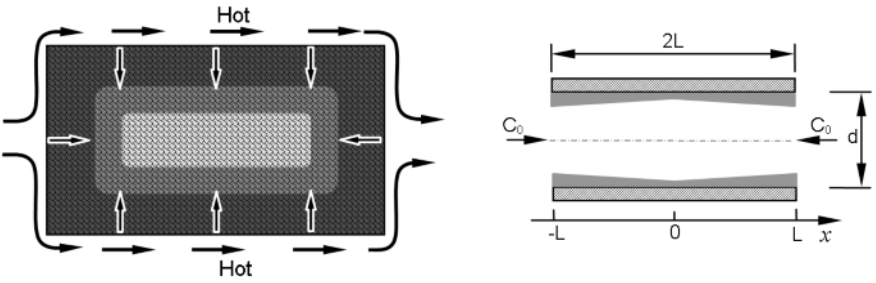

Figure 5.3. I-CVI model: (a) overall model and (b) one-dimensional model

ceramic matrix on the surfaces of the fibres. Therefore, the densification occurs preferentially near the outer surface of the preform because the concentrations of the reactant gases are at their maximum values near the outer surface and decrease along the infiltration direction of the preform. The primary objectives of the I-CVI processes are to maximise the densification rate and minimise the density gradients within the composite so that the mechanical properties of the finished product are consistent throughout its structure. Unfortunately, there is an inherent competition between the deposition reaction and the mass transport of the gaseous species [9]. Rapid deposition reactions result in severe density gradients from the external region to the interior region of the preform, which slows down the deposition rate. An alternative slow-deposition reaction leads to a denser composite but at the cost of an uneconomically long densification time.

Fibre preforms generally have a complex pore size distribution, which may consist of several size ranges, depending on the architecture of the preform. For two-dimensional (2-D) preforms with carbon cloth stacked together the fibres with a diameter of 5~15 μm are arranged in bundles of 500 to 3000 or more fibres. The typical pore sizes between individual fibres are the smallest, on the order of 1 to 10 μm. Pores between the fibre bundles are much larger, up to several hundred, micrometres, and pores between layers of cloth are similar or slightly larger.

To understand the I-CVI process, a one-dimensional model is widely used to demonstrate the principle as shown in Figure 5.3b. Based on this simple schematic diagram, it is possible and essential to establish its process model under steady conditions. A mass-conservation equation model is established based on the fundamental conservation of matter as this lies at the heart of all CVI processes. Under steady conditions the governing transport-reaction equation is written as [12–14]

$$D_e \frac{d^2C}{dx^2} + u\frac{dC}{dx} = rS \tag{5.2}$$

where C is the concentration of a chemical species, D_e is the efficient diffusivity, u is the gas velocity in the x-direction, r is the mol deposition rate per unit of solid surface area and S is the solid surface area per unit volume.

The two terms on the left-hand side of this equation are the net fluxes of the gaseous species into a specific volume by diffusion and convection respectively;

the term on the right-hand side is the deposit production through chemical reactions within the specific volume.

For isothermal/isobaric CVI processes there is no forced flow, i.e. the convection term cannot be taken into consideration. Assuming the first-order reaction, Equation (5.2) becomes

$$D_e \frac{d^2C}{dx^2} = \frac{4}{d}kC \tag{5.3}$$

where k is the first-order reaction constant and d is the diameter of the pore.

The associated boundary conditions for the problem may be explained in the following physical sense. At the exterior surface of the pore the reactant concentration equals the bulk concentration of the gaseous species; at the central cross-section of the pore, considering the symmetric demand, there is no reactant concentration gradient, i.e.

$$X = 0,\ C = C_0 \tag{5.4}$$

$$X = L,\ \frac{dC}{dx} = 0 \tag{5.5}$$

Solving Equation (5.3) gives the concentration profile, $C(x)$, of the precursor species along the pore expressed by

$$C(x) = C_0 \frac{\cosh(\theta \frac{x}{L})}{\cosh\theta} \tag{5.6}$$

where θ is called the Thiele number. θ is a dimensionless parameter and is defined as the ratio of the chemical reaction rate to the mass transfer rate [15]. Furthermore, θ^2 is known as the second Damkijhler number (Da_{II}).

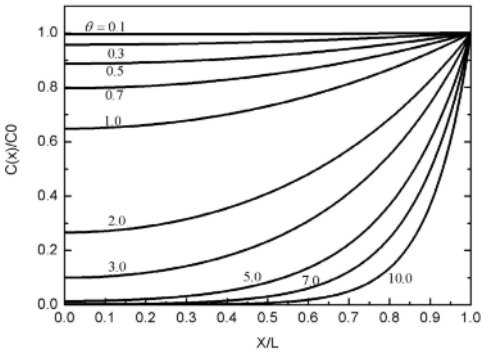

Figure 5.4. Influence of θ number on concentration profile

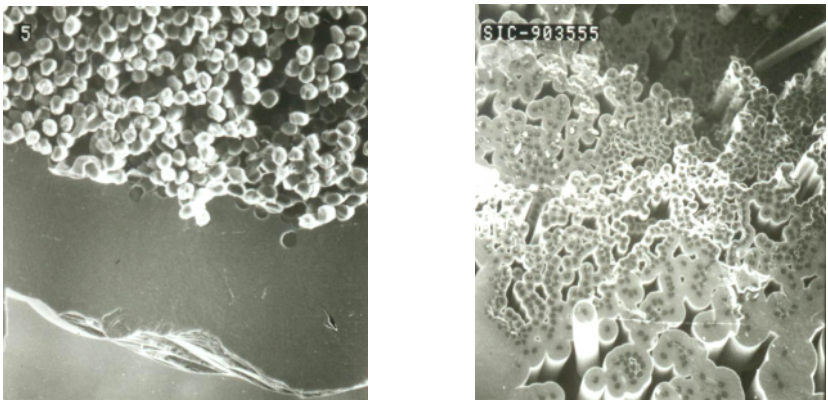

(a) (b)

Figure 5.5. The influence of θ on SiC infiltration: (a) uniform infiltration at small θ and (b) poor infiltration at large θ

$$\theta = (\frac{4kL^2}{dD_e})^{1/2} \tag{5.7}$$

The relationship between the θ value and the concentration is illustrated in Figure 5.4. It is clear that the concentration of the precursor gas decreases with the distance from the opening of the pore. The curve of the concentration distribution is relatively flat when θ is small. However, the curve becomes very steep when the value of θ is greater than 1. Based on the kinetic discussion in Section 4.3.4, the densification process is changed from the chemical reaction regime to the mass transport regime with an increase of the θ value. For the large θ case densification only occurs near the external region of the pore but much poorer densification in the interior region. For small values of θ (< 0.5) the deposition takes place in a kinetics limited region and the infiltration is relatively uniform, which is determined by the uniform distribution of $C(x)/C_0$ along the pore depth.

According to Equation (5.7) the increase in processing temperature and preform thickness leads to larger values of θ and poor density uniformity. As stated previously, CVI processes preferably operate in a chemical-reaction-controlled regime where the ratio of k/D is small. For Fick diffusion, discussed in Section 2.3.1, the diffusivity D is inversely proportional to the pressure and thus operates at lower pressures. Furthermore, coarser pore structures correspond to more uniform deposition. Figure 5.5 shows the microstructures of C/SiC composites prepared at different θ numbers.

As reported by Fedou [16] on SiC infiltration into a pore 10 mm deep and 34 μm in diameter, at a pressure of 20 kPa and with an H_2/CH_3SiCl_3 ratio of 5, the temperature has a significant influence on densification, as shown in Figure 5.6. At temperatures of 950°C, 1050°C and 1100°C, the thickness of an SiC deposit decreases considerably along the depth of the pore in each case. As the processing temperature increases, the profile of the deposit thickness becomes much steeper.

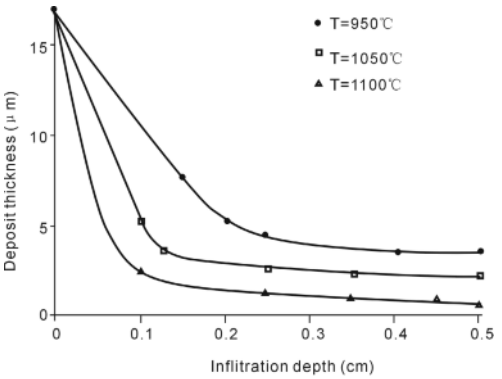

Figure 5.6. Influence of temperature on the thickness profile of SiC infiltration [16]

The figure also shows that the deposition gradient exists under any conditions. These experimental results agree with the theoretical calculations from the one-dimensional model discussed in Equation (5.6). In order to obtain uniformly dense composite material machining is necessary to open the blocked openings for further infiltration.

For I-CVI processes the overall densification kinetics of a preform with initial density (ρ_0) follows an exponential pattern to a "final" density value (ρ_f) as shown in Figure 5.7, which can be expressed as follows [10]:

$$\rho(t) = \rho_o + (\rho_f - \rho_o)[1 - \exp(t/\tau)] \tag{5.8}$$

where τ is the time constant of the process, which decreases with increasing temperature according to the Arrhenius relationship in the chemical reaction limited regime.

The way to achieve the final required density is through several approximately exponential infiltration steps as shown in Figure 5.7. For I-CVI processes, the

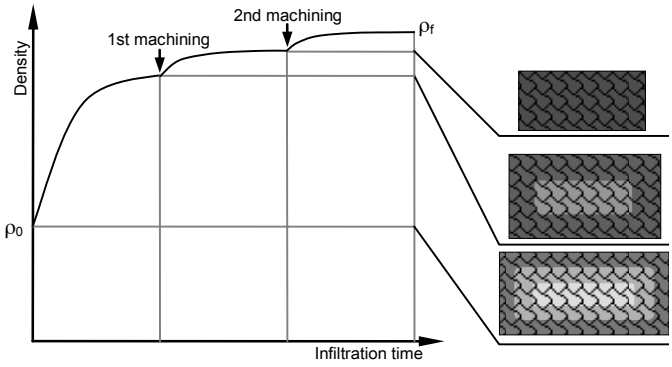

Figure 5.7. Plot of the density of a thick preform against time in an I-CVI process

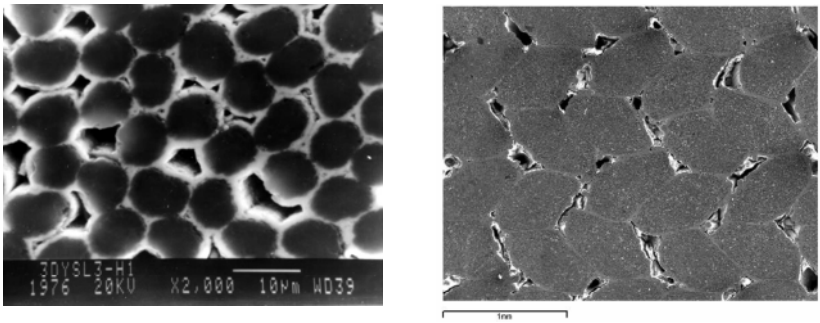

(a) (b)

Figure 5.8. Two kinds of residual pores within the composites by I-CVI: (a) small pores within the bundle and (b) large pores between bundles

diffusion of the gaseous precursors leads to a concentration gradient along the pore, thereby causing blockage of pores due to deposition of a layer of impermeable coating near the opening of the pore. Consequently, the infiltration process must be interrupted to grind off the outer dense layer to enable the reactant gases to penetrate into the interior of the preform. For economical reasons, the infiltration process is normally terminated when the porosity of the composites reaches around 10 to15%. Figure 5.8 shows the typical microstructures of 3-D C/SiC composites. The residual pores include the small pores among the fibres within one fibre bundle and the large pores among the fibre bundles.

From an economical point of view the overall conversion efficiency of the precursor is another important parameter for cost considerations. This efficiency is defined as the ratio of infiltrated mass to the precursor mass introduced into the reaction chamber. Investigations indicate that the conversion efficiency is dependent on the mass transport method, residual time of the precursor, pressure and temperature, etc. As shown in Figure 5.9 the conversion efficiency of propylene (C_3H_6) increases with an increase in residence time but decreases with the partial pressure of the precursor gas. In particular, it is worth noting that the conversion efficiency in the I-CVI process is rather low and generally is in the range of 0.78 to 2.14% [17].

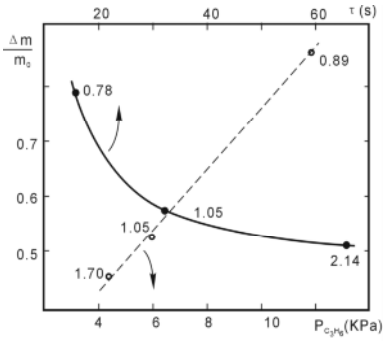

Figure 5.9. Dependence of mass gain on partial pressure and residence time [17]. Note: The numbers next to the data points are conversion efficiencies of C_3H_6

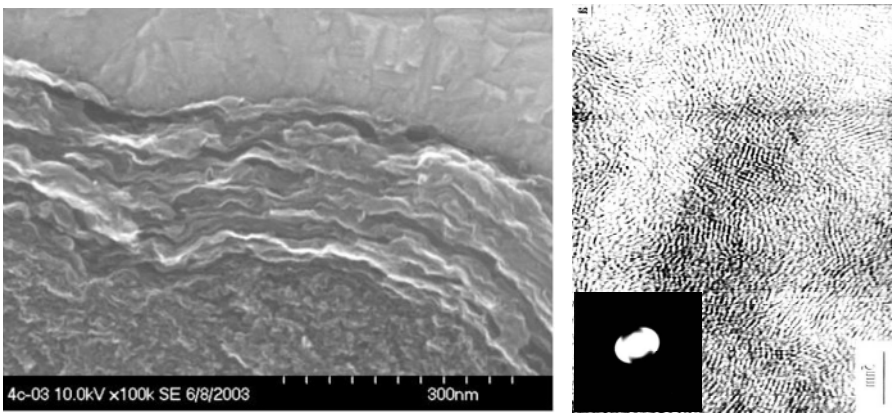

(a) (b)

Figure 5.10. PyC interphase in the C/SiC composites [24]: (a) SEM image and (b) TEM image

5.2.3 Characteristics of Fibre-reinforced Ceramic-matrix Composites

In recent years fibre-reinforced ceramic-matrix composites have been designed and manufactured as very interesting structural materials because of their higher performance at elevated temperatures compared with super-alloys and higher fracture toughness compared with monolithic ceramics. They can be used as component materials in ultra-high-temperature environments, such as advanced aero-engines, scramjet and a thermal protection system for the space shuttle. To date, for example, both carbon-fibre- and silicon-carbide-fibre-reinforced silicon carbide composites (C/SiC and SiC/SiC) have been well developed to serve these purposes.

It is well recognised that the interphase plays a very important role in ceramic-matrix composites [18–21]. The material becomes much tougher if the bonding between the fibre and matrix is neither too strong nor too weak. The interfacial bonding could be tailored with the interphase layer between the fibre and the matrix. The interphase usually performs several key functions: load transfer, matrix crack deflection (mechanical fuse function) and diffusion barrier. The best interphase materials might be those with a layered crystal structure [22, 23], such as hexagonal carbons (pyrocarbons, or PyC), hexagonal boron nitride and multilayered microstructure (such as PyC/SiC/…, BN/SiC/…).

Figure 5.10 shows the microstructure of a pyrocarbon interphase in C/SiC composites.

Figure 5.11 shows the typical failure behaviour of 3-D C/SiC composites, which is quite different from that of monolithic ceramics. The present composite materials exhibit a non-catastrophic failure behaviour and a remarkable failure displacement of around 1.2 mm.

In general the strength of monolithic ceramics decreases significantly at elevated temperatures due to the softening and sliding of a glass phase at the grain

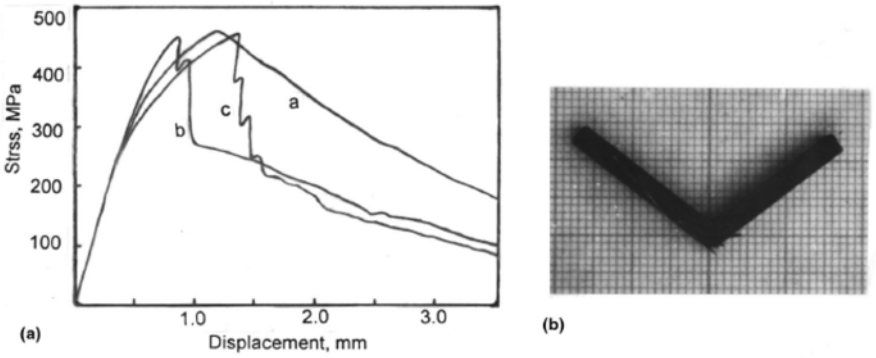

(a) (b)

Figure 5.11. Fracture behaviour of 3D C/SiC composite from RT to 1600°C [24]: (a) stress-displacement curve and (b) fracture surface

boundary. For C/SiC composites fabricated with CVI there is no glass phase in materials. Hence, the flexural strength of the composites does not decrease at temperatures up to 1600°C. The average value of flexural strength is 441 MPa at room temperature, 450 MPa at 1300°C, and 447 MPa at 1600°C. However, the failure behaviour of the composites varies with temperature. This is caused by the thermal stress variation in the composites, which results from the differences in thermal expansion coefficients between the fibre and the matrix. The T300 carbon fibre by Toray Carbon Co., Japan, is an anisotropic material and usually characterised by two thermal expansion coefficients (TECs) [25], a radial TEC (7.0×10^{-6} K^{-1}) and a longitudinal TEC (0.1 to 1.1×10^{-6} K^{-1}). The TEC of a CVI SiC matrix is 4.8×10^{-6} K^{-1} [26]. The interfacial bonding changes from tensile stress to compressive stress as the testing temperature increases to 1300°C, resulting in different failure behaviours of the composites, as shown in graphs a–c in Figure 5.11.

The toughening mechanism of fibre-reinforced ceramic-matrix composites is due to the pull-out phenomenon of the fibre from the matrix. For 3-D C/SiC composites three kinds of pull-out are observed from the fracture, namely the fibre pull-out, the fibre cluster pull-out and the bundle pull-out illustrated in Figure 5.12a, b and c respectively.

The Weibull modulus (m), an important parameter to determine the reliability of materials, is characterised by the scattering range of the material properties. A large value of m implies high uniformity of mechanical properties, while a small m represents a large scattering range. Figure 5.13 shows the result of a Weibull plot of $\ln(1/F)^{-1}$ versus $\ln\sigma$. It is clear from the figure that the flexural strength of 3-D C/SiC composites also obeys a Weibull distribution. The result is consistent with that of a SiC/TiAl composite [27, 28]. The slope gradient corresponding to the Weibull modulus m in Figure 5.13 is as high as 23.3.

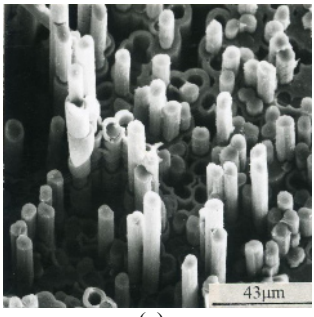

(a)

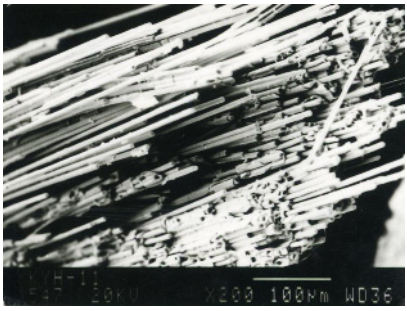

(b)

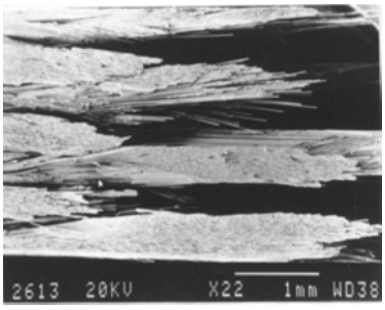

(c)

Figure 5.12. Fracture surface of 3D C/SiC composites [24]: (a) fibre pull-out, (b) fibre cluster pull-out and (c) bundle pull out

The equations for monolithic ceramics together with the experimental results of the notched specimen are used to determine the fracture toughness (represented as K_{IC}) of the 3-D C/SiC composites created with the single edge notched beam (SENB) method. Its value is calculated as 20.3 MPa·m$^{1/2}$, which is much higher than that of monolithic ceramic materials (3 to 5 MPa·m$^{1/2}$). It should be noted that

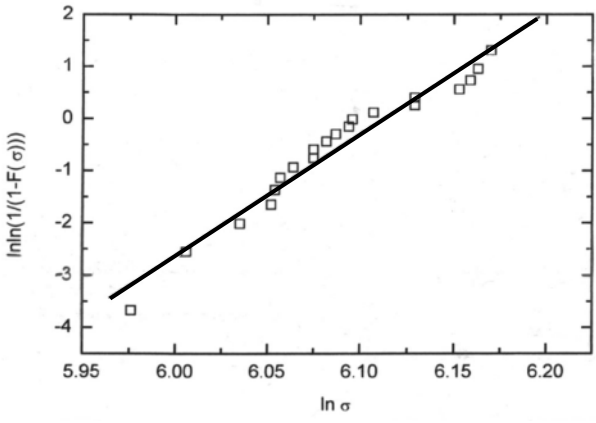

Figure 5.13. Weibull plot for flexural strength of 3D C/SiC composites [24]

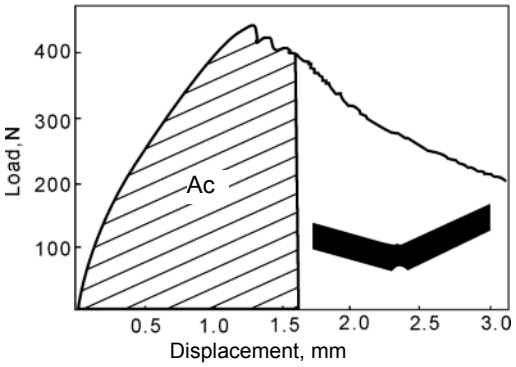

Figure 5.14. Failure behaviour of 3-D C/SiC composite sample with a notch [24]

this value of K_{IC} could not represent the real toughness of present composite materials. The reason for this is that fracture toughness is based just on the linear elastic mechanics for brittle materials, which is not valid and applicable for composites with substantial non-linear behaviour as shown in Figure 5.14.

Instrumented Charpy impact tests on unnotched samples are conducted to determine the energy absorbing capability and dynamic fracture behaviour of the C/SiC composites. The dynamic fracture toughness (αk) is calculated using the following equation:

$$\alpha_k = \frac{\Delta W}{bh} \tag{5.9}$$

where ΔW is the absorbed energy of materials during impact testing and b and h are the thickness and width of a specimen respectively.

For 3-D C/SiC composite materials the value of α_k is 62 kJ·m^{-2}, which could be comparable to that of a super-alloy (α_k = 80~160 kJ·m^{-2}). The impact fracture

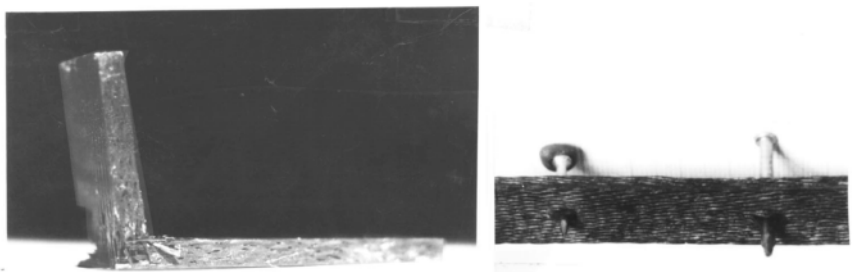

(a) (b)

Figure 5.15. Impact fracture surface of C/SiC composites [24]: (a) after Charpy impact test and (b) after the nails penetrated test

surface is shown in Figure 5.15. It is worthwhile to note that the materials are still connected together, not broken into pieces, after the impact tests. In addition, the composites could also be penetrated by a steel nail without any severe fracture, as shown in Figure 5.15b, showing a strong reliability. Overall, C/SiC composite materials exhibit excellent toughness characterised by insensitivity to cracks, non-catastrophic failure behaviour and high reliability.

5.2.4 Isothermal and Isobaric Chemical Vapour Infiltration Applications

As a well-established and relatively well-understood technique I-CVI is still widely used in both the laboratory and industry. Uniform temperatures and pressures within the reactors can be easily realised in practice and make it suitable for industrial manufacturing. So far, very large reactors (up to 2500 mm in diameter) have been successfully designed and developed for densification of C/C, SiC and other refractory composites [29].

I-CVI has been widely used to manufacture carbon/carbon braking disks since the 1960s. In a common application as shown in Figure 5.16, multicylindrical carbon brake disk preforms, typically 550 mm in outer diameter and 20 to 30 mm in thickness, are placed in a hot-wall reactor at a temperature of 1000°C and exposed to the CH_4 precursor at a pressure of 1to 30 kPa [29].

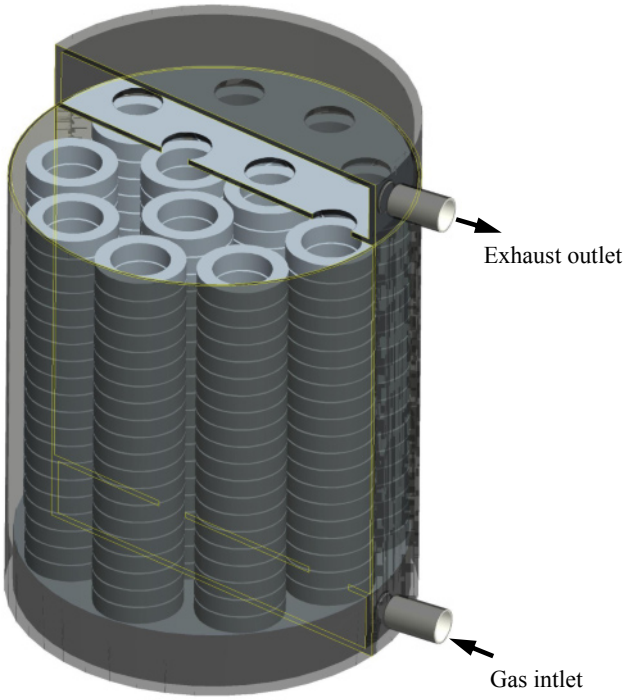

Figure 5.16. A large I-CVI reaction chamber for C/C braking disk densification

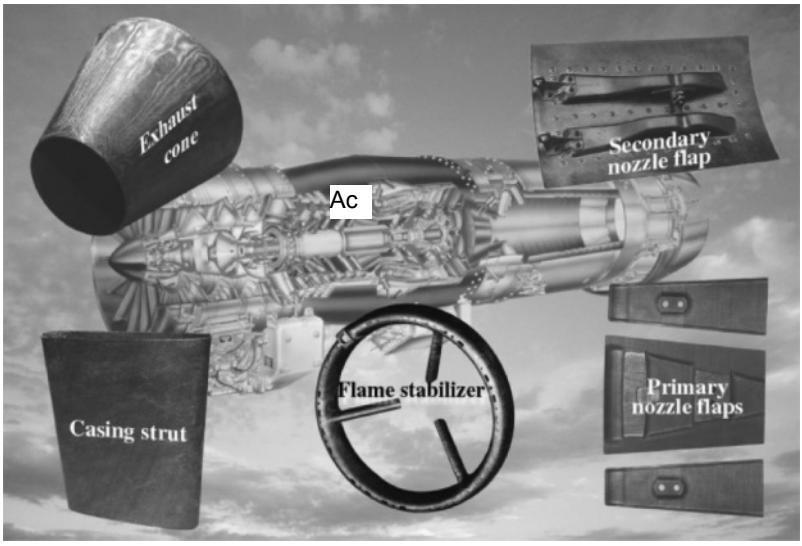

Figure 5.17. Potential applications of SiC-matrix components in aero-engines [33]

Due to the excellent aforementioned properties, fibre-reinforced ceramic-matrix composites have been identified as improving the thrust-to-weight ratio of higher performance aero-engines. Some typical projects include integrated high-performance turbine engine technology, high-speed civil transport, propulsion system in high-speed research (HSR), the continuous fibre ceramic composite programme in USA [30], the novel ceramic composites project in European as well as the research institute of advanced material gas generator in Japan [31]. The potential applications are nozzle flaps, exhaust cone, flame stabiliser, combustion liners and turbines. As presented in Figure 5.17 C/SiC flaps have been manufactured using an I-CVI technique in volume production by a company called Snecma and they have been successfully used in M-88 aero-engines for Rafale fighters since 1996. By using C/SiC composites the flaps save 50% of the weight compared with the original material super-alloy Inconel 718 [32, 33]. C/SiC and SiC/SiC composites have also been demonstrated for use in thermal protection systems for the space shuttle and scramjet engines [34].

5.3 Thermal Gradient and Forced Flow Chemical Vapour Infiltration

5.3.1 General Description

In a forced flow CVI (F-CVI) process, the precursor gases are allowed to flow through the fibre preform, rather than relying on diffusion transport as with I-CVI processes. An F-CVI process offers the advantages of much reduced processing

time, improved infiltration efficiency and hence economics, especially for components with thick sections.

A schematic diagram of F-CVI equipment is shown in Figure 5.18 [6]. The fibrous preform is placed in a water-cooled metal holder which cools the bottom and sides surrounding the preform to prevent undesirable deposition there. The top of the preform is heated by a heating element. As a result the temperature gradient is built up within the preform. The precursor gases are forced to flow through the preform from the cold surface to the hot surface. The back pressure of the precursor gases is in a range of 0.1 to 0.2 MPa. In this case a pressure gradient has

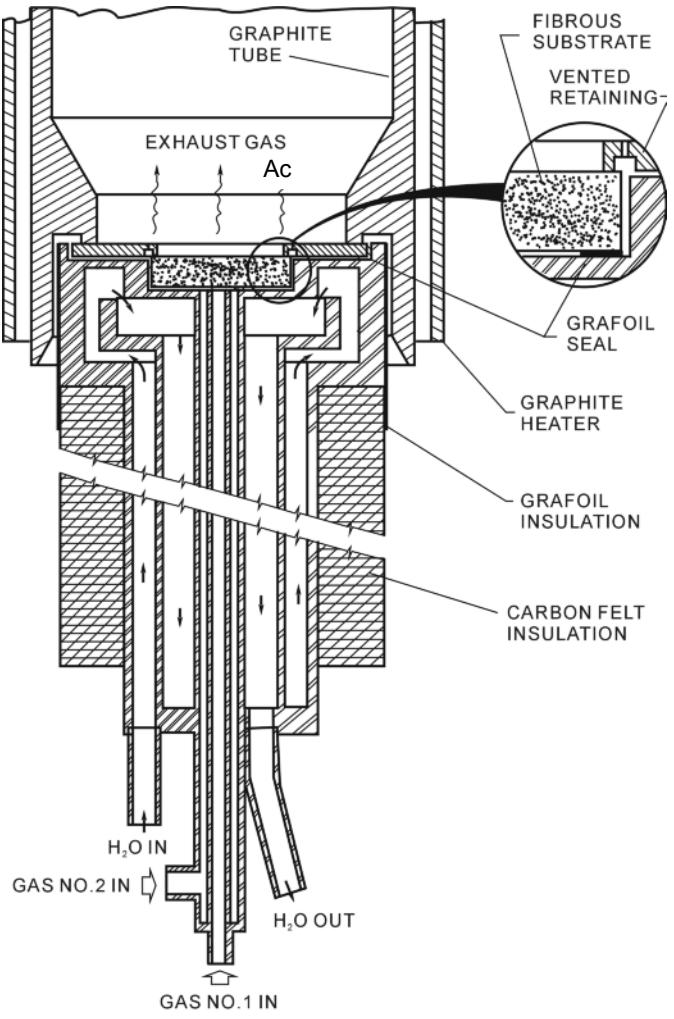

Figure 5.18. Schematic of F-CVI process for plate preform [6]

the opposite direction to the temperature gradient. The infiltration occurs progressively from the top to the bottom of the preform.

Grafoil is used to seal the gaps between the preform and the holder. When the top surface region becomes dense, the gases flow up into the preform, then penetrate radially through the preform to the annular void space around the preform and finally flow out through the vented retaining ring.

The F-CVI process can also be used to infiltrate tubular preforms radially by creating a thermal gradient from the inside of the tube to the outside. As shown in Figure 5.19, the outside of the preform is heated while the cold water is circulated through the stainless steel injector to cool the inside of the preform. The precursor gases flow up in the gas guide pipe which is connected to the gas distributor. The gases are then forced to flow radially through a number of holes on the distributror and further penetrate uniformly through the preform along the longitudinal direction. The preform is supported by the mandrel. The gases are finally guided to the reactant gas outlet after passing the mandrel.

In order to demonstrate the ease of scaling this process to fabricate much larger work pieces Besmann *et al.* [36] developed a large F-CVI system at the Oak Ridge National Laboratory, USA, as shown in Figure 5.20. The furnace shell and lid are water-cooled. The top lid needs to be raised by pneumatic lifters. There are two

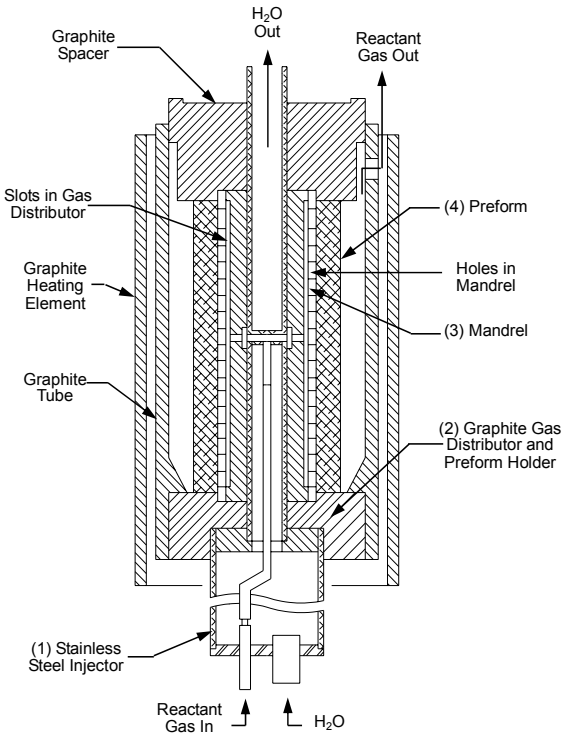

Figure 5.19. Schematic of F-CVI process for tubular preform [36]

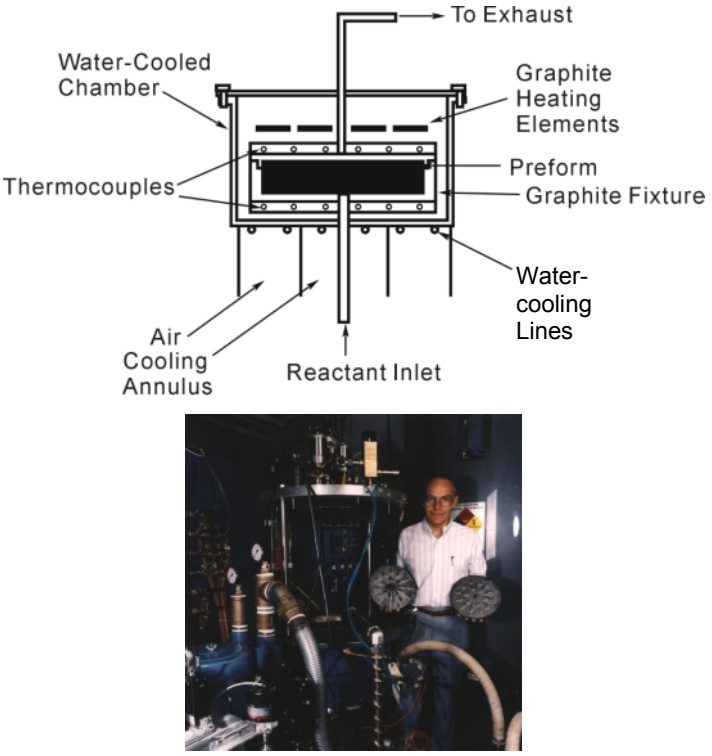

Figure 5.20. F-CVI furnace for large-scale component fabrication [37]

concentric heating elements which are controlled independently and, therefore, allow good radial temperature uniformity. The radial temperature difference can be controlled to less than 10°C. The fibre preform is placed in the fixture. The fixture also acts as a reaction chamber with a good seal to prevent precursor gases leaking out of the fixture. The reactant gas is introduced by an inlet fitted into the bottom of the fixture, while the exhaust exits the fixture through a graphite tube and then to the metal exhaust line. The effective working capacity of the fixture is 300 mm in diameter and 24 mm thick.

The bottom surface of the F-CVI chamber is cooled either with a water-cooled plate or with forced air. A baffle is designed to direct the air flow to varying degrees into the inner or outer annulus, thus controlling the lower surface radial gradient. Thermocouples are placed above and below the preform fixture to measure the temperatures, which are maintained by controlling power to the heating elements based on the signals from the control thermocouples on the hot side and the positioning of the air flow baffle on the cool side. The size of the preform reported in the researchers' work is 246 mm in diameter and 12.7 mm thick with a 12.7-mm-diameter central hole. The fibre volume fraction of the preform is 33%. During the infiltration process the flow rates of CH_3SiCl_3 and H_2 are 5 g·min^{-1} and 5 l·min^{-1} respectively; the hot surface temperature of the preform is 1200°C and an infiltration time of 40 h is required for each run.

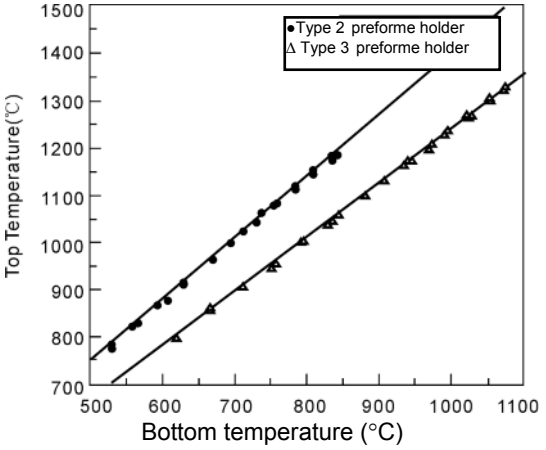

Figure 5.21. Temperature profile within the preform for F-CVI process [38]

The temperature gradient is dependent on the configuration of the preform holder which determines the cooling effect. For a fibre preform with a thickness of 8 mm the temperature profiles are measured at the top and the bottom of the preform without infiltration, as shown in Figure 5.21. The temperature differences between the top surface and bottom surface of the preform are around 350°C and 250°C, corresponding to preform holders 2 and 3 respectively.

In contrast to the I-CVI technique, processing parameters must be adjusted during the F-CVI process. An example for F-CVI C/C is given by Vaidyaraman *et al.* [38]. The pressure above the preform is atmospheric pressure (or slightly higher than atmospheric pressure). At the initial infiltration stage, the pressure in the precursor supply line is 3.4 kPa above atmospheric pressure. This pressure gradient forces the precursor gases to flow through the preform. The reagent gas first comes in contact with the cooler side of the preform then flows up through the preform to the hot side. As the infiltration progresses, it is necessary to increase the back pressure in the supply line because the preform becomes denser. A higher pressure is required to force the gases to flow through it. The infiltration process typically ends when the back pressure on the cold side of the preform increases about 170 kPa.

5.3.2 Forced-Flow-Chemical Vapour Infiltration Model

For the F-CVI process shown in Figure 5.22a a temperature gradient is applied across the preform thickness and the precursor gases are forced to flow through the preform from the cold to the hot surface. It is desirable to obtain uniform deposition throughout the preform; this can be accomplished by choosing and controlling the precursor pressure and processing temperature. A high precursor concentration on the cold side compensates the lower temperature, and a lower concentration at the hot side offsets the higher temperature combining these results in a uniform deposition along the thickness of the preform.

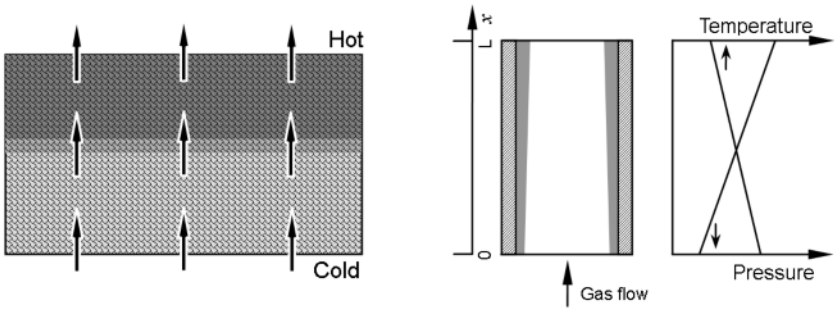

(a) (b)

Figure 5.22. F-CVI model: (a) overall model (b) one-dimensional model

In practice a faster deposition process occurs in the hot region of the preform compared with the cold region of the preform. Figure 5.22b shows the effect of coating thickness on temperature. In addition, the temperature gradient helps to prevent the formation of an impermeable skin. This is due to the fact that the preform is exposed to the precursor gases in the low temperature region first. This approach allows the process to be conducted at much higher temperatures (around 200°C) than I-CVI processes, thereby further reducing the processing time significantly. F-CVI also offers greater flexibility in the selection of processing conditions. It is not essential to use low temperatures, pressure and precursor concentration as in I-CVI processes. Consequently, there is a wider range of selection of the conditions under which deposits possessing the required microstructure and properties can be obtained.

By forcing the precursor gases through the preform, the diffusion term in Equation (5.2) can be neglected, and the governing transport-reaction equation is rewritten as

$$u\frac{dC}{dx} = RS \tag{5.10}$$

The associated boundary conditions are given by

$$x=0,\ C=C0 \tag{5.11}$$

The concentration of the precursor along the pore can then be obtained as

$$C(x) = C_0 \exp(-Da_I \frac{x}{L}) \tag{5.12}$$

where the cold surface of the preform is at $x = 0$; the concentration of the precursor gases depends on the dimensionless parameter, Da_I:

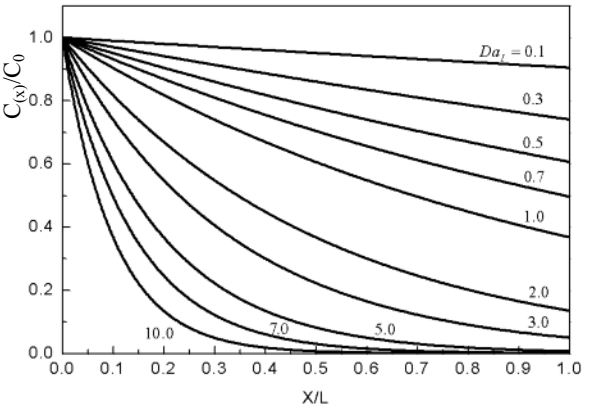

Figure 5.23. Relationship of Da_I number and concentration distribution

$$Da_I = \frac{kSL}{u} \tag{5.13}$$

where Da_I is called the first Damkijhler number. It represents the ratio of chemical reaction rate to the convective mass transfer rate.

As shown in Figure 5.23, the concentration profile of the precursor gas is related to the value of Da_I. The concentration gradient of the precursor gas becomes steeper with increasing Da_I. Due to complex coupling effects between the pressure and temperature of F-CVI it is very difficult to model this phenomenon. A large body of research work has been undertaken under isothermal conditions to simplify the simulation. Under isothermal conditions the concentration profile represents the deposition gradient. In such a case densification always occurs more rapidly at the precursor gas entrance region of the preform.

In order to obtain a uniform infiltration, Da_I should be as small as possible. Processing conditions must include a large gas velocity (large pressure gradient) and large pore diameter, but with a short pore length (preform thickness). Moreover, the increase in the gas velocity through the increase of the total gas flow rate will enhance both uniform and rapid matrix deposition. Hence, the suitable selected processing parameters can achieve the maximal densification rate and the minimal density gradient. This is a distinguishing feature aided by the use of forced gas flow, which is different from that of I-CVI techniques based on mass diffusion.

F-CVI processes take place far from the thermodynamic equilibrium. The dimensionless Peclet number, *Pe*, is used to describe this process [39]:

$$Pe = \frac{uL}{D} \tag{5.14}$$

The Peclet number means the ratio of the mass transfer rate by convection mechanism into the pore to the mass transport rate by a diffusion mechanism. At

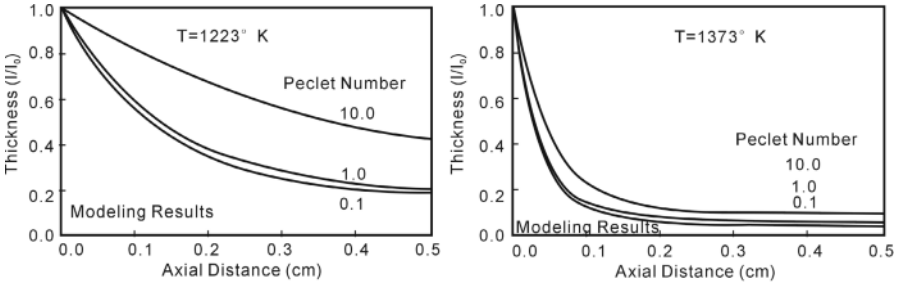

(a) (b)

Figure 5.24. Forced-flow effect on the infiltration profile [39]: (a) at 1223°K and (b) at 1373°K

low Pe numbers the mass transfer is dominated by a diffusion mechanism, whereas at large *Pe* numbers convection is dominant.

Figure 5.24 shows the simulated results of F-CVI under isothermal conditions. The forced effect on infiltration is very limited if the Pe number is small. Uniform infiltration is obtained when the Pe number reaches 10 at relatively the low temperature of 1223°K. The reason is the convective flow can force much more gaseous species to penetrate deeply into the pores of the preform. However, the influence becomes minimal at high temperatures (1373°K) even for high a Pe number (10.0).

5.3.3 Characteristics of Forced-Flow-Chemical Vapour Infiltration Composites

For an I-CVI process the surfaces of preforms require grinding in several stages during a complete process in order to open the blocked channels or pores in the outer region of the preform for further infiltration. In contrast, F-CVI is a one-step

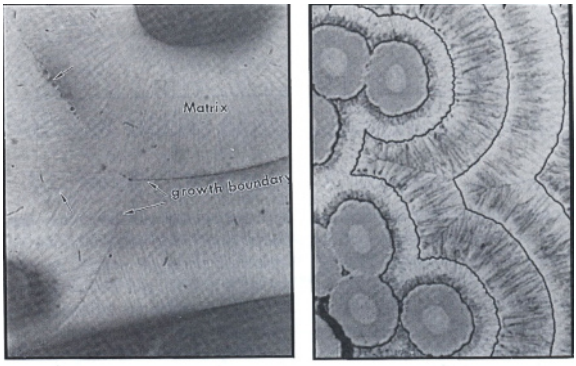

(a) (b)

Figure 5.25. Microstructure comparison between I-CVI and F-CVI processes [40]: (a) F-CVI and (b) I-CVI

processing method, which implies that the infiltration of the composites could be realised in only one run. Figure 5.25 shows the microstructures obtained by F-CVI and I-CVI techniques respectively. In both cases, SiC is deposited on the fibre surface, then grows radially until it meets another growing deposit. Multistage infiltration in an I-CVI process results in a multilayered structure, which is very similar to the growth rings of a tree.

It has been reported [40] that the infiltration rate of F-CVI can reach 1 mm per hour, while the infiltration rate of I-CVI techniques is much slower, around 1 mm per day. Figure 5.26 shows the density distribution of a large disk fabricated using a F-CVI technique for 40 h. The dimension of the SiC/SiC composite disk is 264 mm in diameter and 12.7 mm thick. The results indicate that the relative densities (real density/theoretical density) of the interior region are high, around 90%. However, the relative density of both exterior parts is lower (about 80%) than that of the central part.

Investigations reveal that the precursor conversion efficiency is dependent not only on the nature of the precursor but also on the processing conditions such as

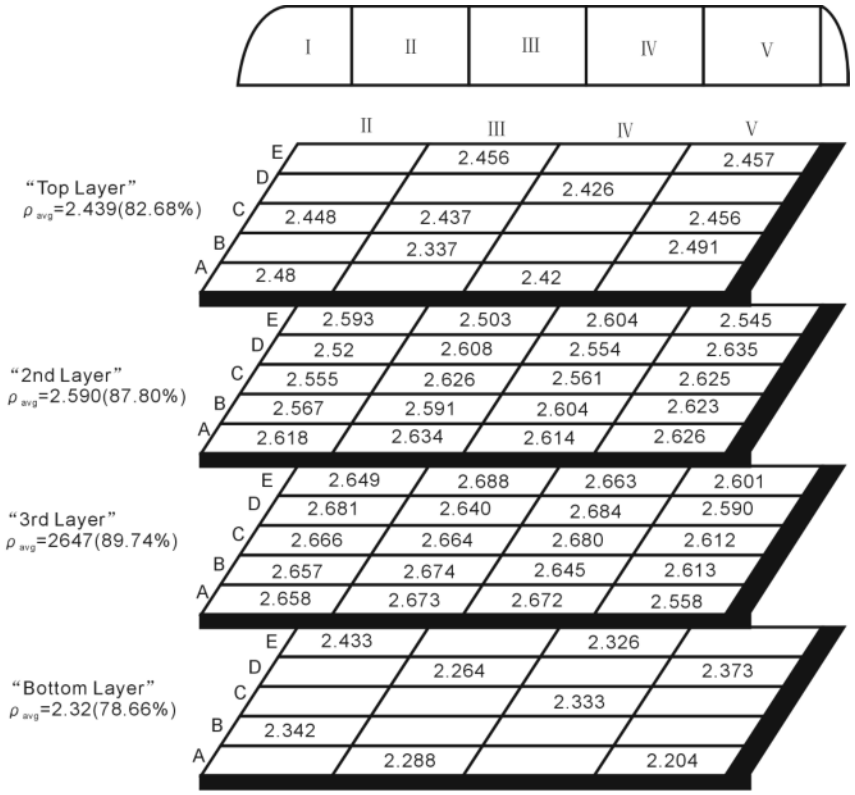

Figure 5.26. Density distribution within a large Nicalon/SiC disk [37]

mass transport method, temperature and pressure of the process, etc. The precursor conversion efficiency in F-CVI processes is much higher than that in I-CVI techniques [38]. For the F-CVI process the observed conversion efficiencies are 5~24% for C_3H_6, 3~14% for C_3H_8, and 10~15% for CH_4. However, the efficiency is typically 0.8~1.5%, reported for isothermal and isobaric CVI techniques.

5.4 Thermal Gradient Chemical Vapour Infiltration

5.4.1 General Description

Both experimental and simulated results of CVI processes reveal that the infiltration rate could be significantly increased with temperature gradient, even as low as 5%, exerted along the thickness of the preform [41]. The direction of the temperature gradient is opposite to that of the concentration gradient of the precursor. Under such conditions an in-depth infiltration is favoured and the densification front moves from the inner sections of the pore towards its entrance. As a result, a complete infiltration is achieved without any early pore sealing.

As shown in Figure 5.27 the I-CVI process is performed in a hot-wall reactor, in which both the heat and mass are transferred from the outer region to the inner region of the preform. As a result it leads to a severe density gradient and forms an impermeable "skin" which impedes the further densification of the inner part of the preform. However, thermal gradient CVI (TG-CVI) is a cold-wall technique, although the densification is also dependent on the mass diffusion. A temperature gradient can be deliberately established across the fibre preform. Unlike the I-CVI model, TG-CVI has a mobile infiltration front within the preform, caused by a

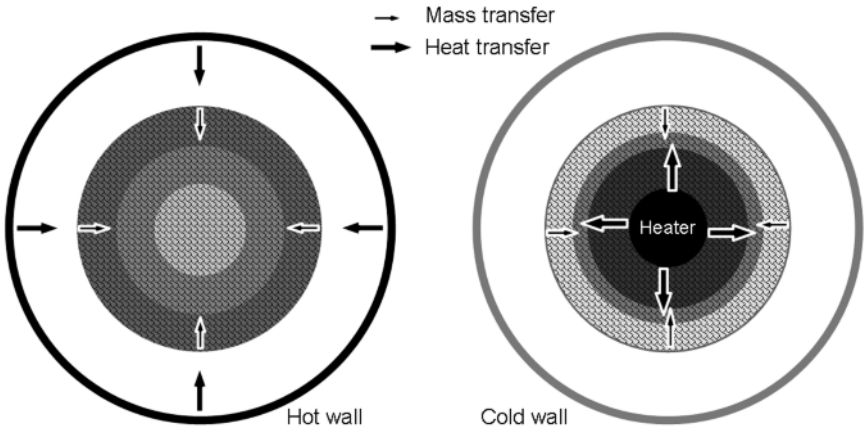

Figure 5.27. Schematic comparison of the I-CVI and TG-CVI techniques: (a) I-CVI and (b) TG-CVI

temperature gradient as shown in Figure 5.27. The direction of the mass transport is opposite to that of the heat transfer. In this case, there is no coupling between the mass transport and chemical reactions [42]. Therefore, the chemical reactions take place in the exact position needed at relatively high temperatures. In this way, the infiltration front moves progressively from the interior region to the exterior region within the fibre preform. If there is a steep temperature gradient, the infiltration rate of TG-CVI is about one or two orders of magnitude larger than that of isothermal/isobaric CVI. TG-CVI is especially suitable for the fabrication of annular and cylindrical preforms.

5.4.2 Some Typical Thermal Gradient/Isobaric Chemical Vapour Infiltration Techniques

5.4.2.1 Inductive Heating Thermal Gradient Chemical Vapour Infiltration

Since its inception, the TG-CVI technique has received considerable attention. During the 1970s this method was developed to manufacture carbon/carbon composites in rocket components reported by Buckley [43] and Stoller *et al*. [44]. As shown in Figure 5.28 the carbon fibre preform is placed over a conical graphite substrate, which is also used as induction susceptor to heat the preform. As reported by Lieberman *et al*. [45] the free space between the sleeve and the preform is about 25 mm. At the beginning of the infiltration stage the carbon preform does not couple electromagnetically to the coil because its density is very low, 0.14 ± 0.02 g/cm^3. As a result the pyrocarbon is only deposited on the surface of the preform very close to the susceptor and the deposition front moves outwards radially through the preform as the densified preform becomes inductively heated.

The TG-CVI process takes place at a temperature of 1325°C (mandrel temperature) and pressure of 630 Torr. Methane is used as precursor gas and its

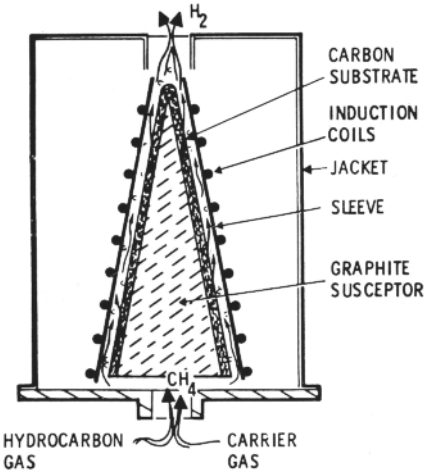

Figure 5.28. Schematic diagram of TG-CVI for conical component [43]

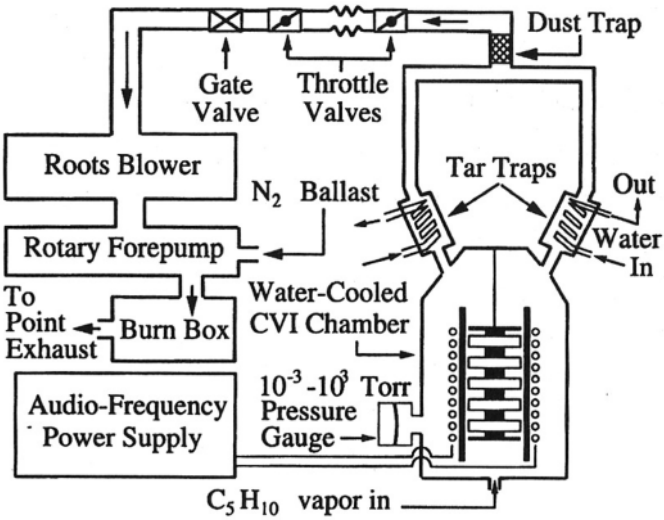

Figure 5.29. Schematic of TG-CVI system developed by AlliedSignal [10]

flow rate is 61 l·min^{-1}. Argon is used as diluent gas at a flow rate of 205 l·min^{-1}. This process has a disadvantage of forming soot, due to the combination of very high temperature and high pressure caused by homogenous nucleation in the gaseous phase. There is a density gradient from the inner region (1.74 to 1.84 g·cm^{-3}) towards the outer region (1.87 to 1.89 g·cm^{-3}) of the cross-section of the carbon/carbon composites.

In order to infiltrate thick carbon preforms within a short time in one processing cycle, a novel TG-CVI method was developed by AlliedSignal, Inc. [46], USA. As shown in Figure 5.29 the carbon preform disks are heated by the induction method. The preforms are fabricated with non-woven PAN carbon fibres and have a relatively high density in the range 0.4 to 0.6 g·cm^{-3}. The size of the carbon preform disks is 108 mm (outer diameter, o.d.) × 44 mm (inner diameter, i.d.) × 30 mm (thickness). Carbon fibre preform disks are placed around a mandrel (molybdenum or alumina) and spaced about 10 mm apart. In this case the preforms with high density can couple with the electromagnetic field. Hence, an electrically conductive mandrel is not required for heating. A quartz tube inserted between the carbon preform disks and the inductive coil is used as a flow channel for the precursor gases. The temperatures are measured with Pt-Rh/Pt thermocouples inserted into the disks as well as with a pyrometer through a sapphire window. The processing parameters are defined as follows: power and frequency of induction power supply: 8.8 to 13.2 kW, 4.9 to 8.6 kHz; total pressure: 20 to 100 Torr and cyclopentane (C_5H_{10}); flow rate: 170 to 540 ml·min^{-1}.

This TG-CVI technique allows significantly higher deposition temperatures, around 200°C higher than that of I-CVI techniques. The infiltration process is normally monitored and controlled in real time. The precursor conversion

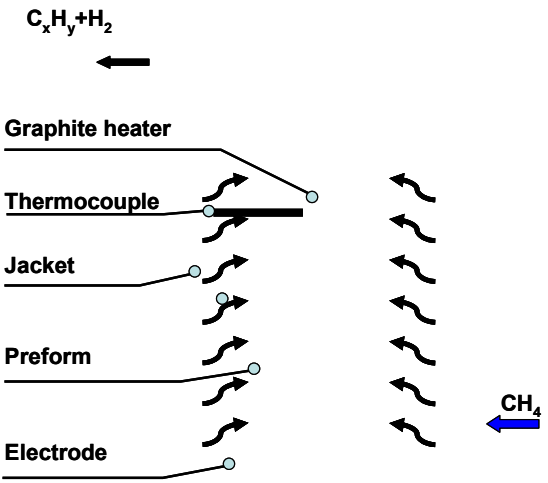

Figure 5.30. Schematic diagram of resistant heating TG-CVI [48]

efficiency is typically 20 to 30% [47]; but very little tar and no soot are produced during the infiltration process. The desirable rough-laminar carbon microstructure is obtained. This technique, therefore, has significant scale-up potential and economic competitiveness in being applied to other materials and wider applications.

5.4.2.2 Resistant Heating Thermal Gradient Chemical Vapour Infiltration

In this approach conductive and refractory materials (e.g. C, Mo or W) are used as the heating element and located at the centre of the preforms. Large electric currents with low voltage flow through the heating element. Hence, a temperature gradient is established with an inside-out direction along the radial direction of the preforms. Figure 5.30 shows the principle of such a resistant heating TG-CVI system with its detailed constituent components.

The following discussion describes a specific example with more detailed information to illustrate the design and operation of such a system [48]. The density of the carbon fibre preform in this case is 0.6 g·cm^{-3} and its size is 160 mm (o.d). × 80 mm (i.d.) × 25 mm (thickness). Carbon fibre preforms are stacked vertically and kept tightly together by a mechanical clamp. Natural gas (mainly containing CH_4: 98%) is used as the precursor gas for infiltration. During the process the densification only occurs in a narrow region where the temperature is sufficiently high for the pyrolysis of the hydrocarbon gas. The temperature gradient within the preform depends on several factors including the heating power, electrical resistance of the heater, the thermal conductivity of the preforms and the cooling of the gas flow along the exterior surface of the preforms. The

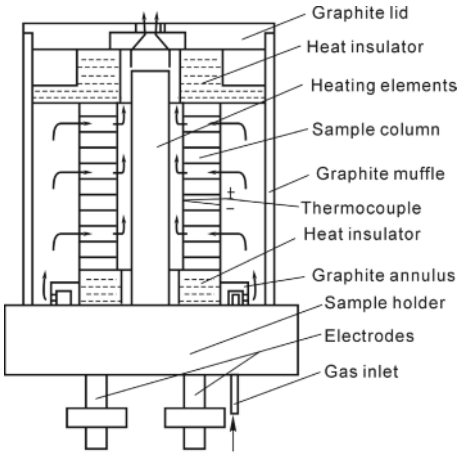

Figure 5.31. Schematic diagram of directional-flow TG-CVI [49]

thermocouple is inserted into the preforms to measure the temperature. The deposition temperature is kept constant by controlling the electrical power supply. During the TG-CVI process the thermocouple is progressively being pulled outwards. The pulling speed of the thermocouple is equal to the moving speed of the deposition front, which is controlled at around 0.25 $mm \cdot h^{-1}$. A schematic diagram of this process is presented in Figure 5.30.

Directional-flow TG-CVI was developed to increase the density uniformity, prevent the formation of a dense crust on the surface of preforms and improve the conversion efficiency of the precursor. In such a developed solution, the precursor gases are only allowed to flow into the carbon preforms in the direction of predefined paths as shown in Figure 5.31.

During the densification process, the preform can be distinctly divided into three zones as shown in Figure 5.32a: the completely deposited zone or C/C composites, the depositing zone and the as-prepared porous preform zone. In Figure 5.32b, there is a steep temperature gradient within the depositing zone, as illustrated in the corresponding density gradients of the preforms. Due to the dynamic nature of the depositing process it is a common practice to link the density gradients to the temperature gradient.

Figure 5.33 shows the microstructure characteristics of C/C composites fabricated by the TG-CVI process. The rough laminar pyrocarbon (RL) is located near the heating source at position 1 in Figure 5.32b and the corresponding microstructure is shown in Figure 5.33a. A mixture of smooth laminar and isotropic structure pyrocarbon (SL+ISO) at position 2 is formed and its microstructure is shown in Figure 5.33b. At and near the depositing zone, the pyrocarbon has a smooth laminar structure (SL), and the related microstructures are shown in Figure 5.33c and d. The structure characteristic of the pyrocarbon is dependent on the deposition temperature, the concentration and nature of the precursor as well as those of intermediates. During the TG-CVI process the width of the depositing zone (δ) depends on the deposition temperature (T_d), the

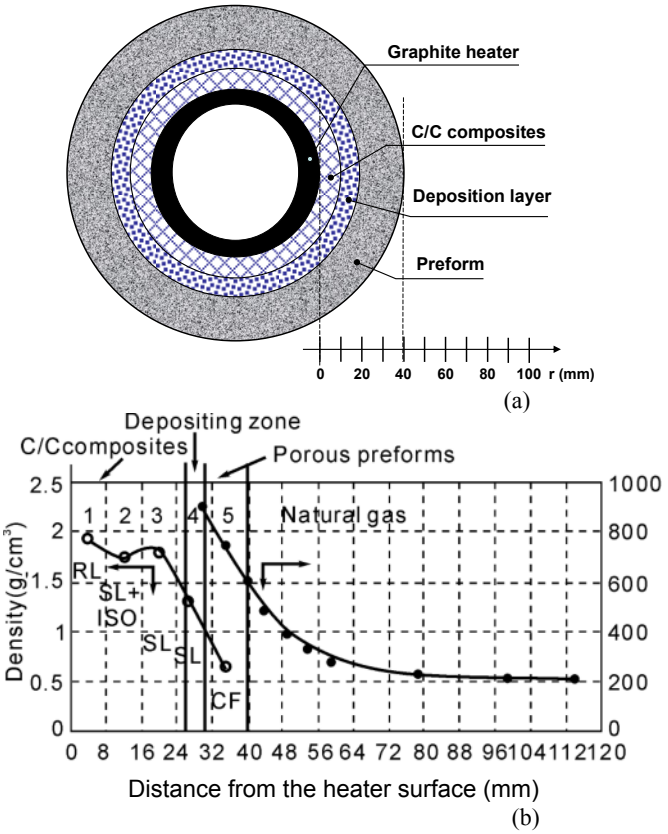

Figure 5.32. Schematic of deposition process and the relationship of distance vs density [48]: (a) different zones and (b) profiles of density and temperature

minimum deposition temperature (T_{min}), and the temperature gradient ∇T within the preform. The relationship is empirically given by [49]

$$\delta = \frac{T_d - T_{\min}}{\nabla T} \tag{5.15}$$

For a given thermal gradient higher deposition temperatures result in a wider depositing zone. In this case the pores are very easily trapped within the composites because of the complex architecture of the preforms and a bottleneck effect for the bottle-shaped pores; this produces poor infiltration for these pores. A relatively low deposition temperature and steep thermal gradient give rise to high density and uniform densification.

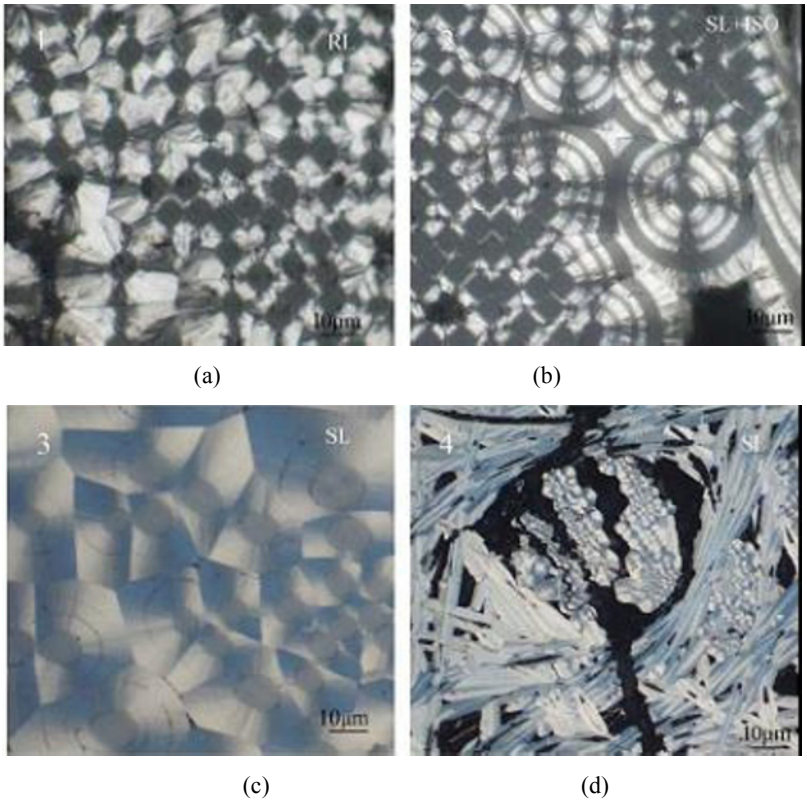

Figure 5.33. Microstructure characteristics of pyrocarbon at the radial cross-section of a preform [48]: (a) RL pyrocarbon at position 1, (b) SL+ISO pyrocarbon at position 2, (c) SL pyrocarbon at position 3 and (d) SL pyrocarbon at position 4

5.4.2.3 Heaterless Thermal Gradient Chemical Vapour Infiltration

For a thick plate carbon preform a steep temperature gradient could be established across the thickness by passing an electric current through it rather than by using a heating element, as shown in Figure 5.34. This kind of method is also called heaterless CVI (HT-CVI) [50, 51]. In this case the highest temperature is at the centre while the lowest temperature is located on the outside surface of the preform. In order to build a steep thermal gradient, some additional methods are used to cool the outer surface of the preform.

As shown in Figure 5.34 a carbon fibre preform with dimensions 380 × 120 mm × 7 mm is directly connected to electrodes by passing through an electric current. Due to the low electric resistance of the carbon preform, it is necessary to use an electric power source with a large electric current (0.45 to 1.10 kA) but at a low voltage (40 to 25 V). The heat generated by the current is proportional to the power of the electric current, hence a large electric current significantly increases the heat produced. After the preform (with a density of 0.6 g·cm^{-3}) is infiltrated

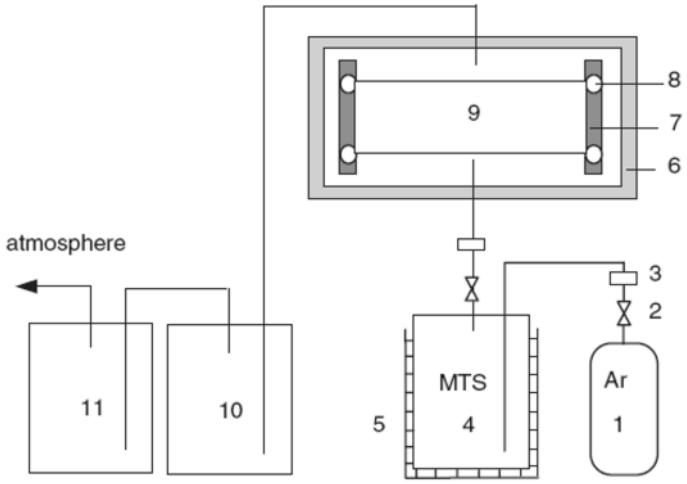

Figure 5.34. Schematic of heaterless TG-CVI process [51] 1: Ar, 2: shut-off valve, 3: mass flow controller, 4: methyltrichlorosilanc (MTS), 5: thermostat bath, 6: water-cooled wall, 7: graphite electrode, 8: graphite bolt, 9: fibre preform, 10: NaOH trap, 11: H_2O trap

with CH_3SiCl_3 and H_2 for 25 h, the density of the C/SiC composite reaches 2.32 g·cm^{-3}. Figure 5.35 shows that the SiC matrix is well infiltrated into the large pores, between the plies and small pores among the individual fibres. From the micrographs, the SiC infiltration rate is calculated with the SiC coating thickness divided by the infiltration time. The maximum infiltration rate within the inter-fibre pores is as high as 0.33 μm·h^{-1}.

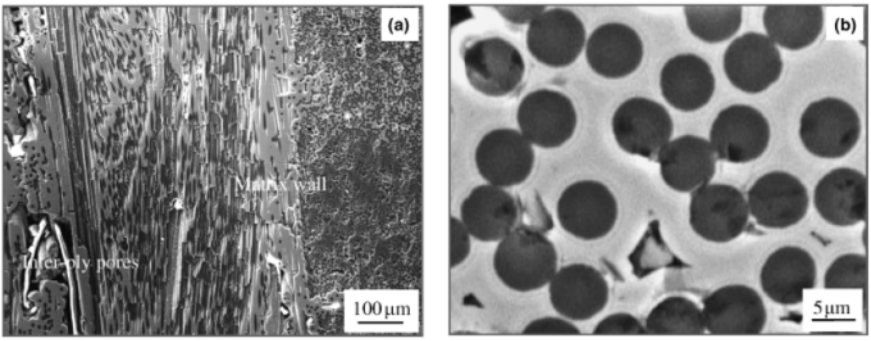

(a) (b)

Figure 5.35. Structure characteristics of HT-CVI C/SiC composites [51]: (a) macro-structure and (b) microstructure

5.4.3 Temperature Profile Within the Preform

As mentioned above both exterior and interior heating sources are methods for creating a temperature gradient within a preform. If the preform is heated with an exterior heating source, the temperature profile within the preform could be treated as a linear distribution according to the Fourier law of heat transfer in Section 2.3. If the preform is heated by itself (as in Section 5.4.2.3), however, the situation of interior heating source is much more complex.

Here we consider a cylinder model as shown in Figure 5.36a. In order to simplify the calculation some reasonable assumptions are made as follows:

1. the cylinder has a large aspect ratio, i.e. $L >> 2R$,
2. both the electric conductivity and thermal conductivity remain constant within the whole temperature range and
3. the outer surface temperature of the cylinder is maintained at constant temperature (T_0).

In steady conditions, the following relation can be established according to the energy balance [12]:

rate of thermal energy in across surface at r	+	rate of thermal energy in across surface at $r+dr$	=	rate of thermal production by electrical heating

The relationship is written as

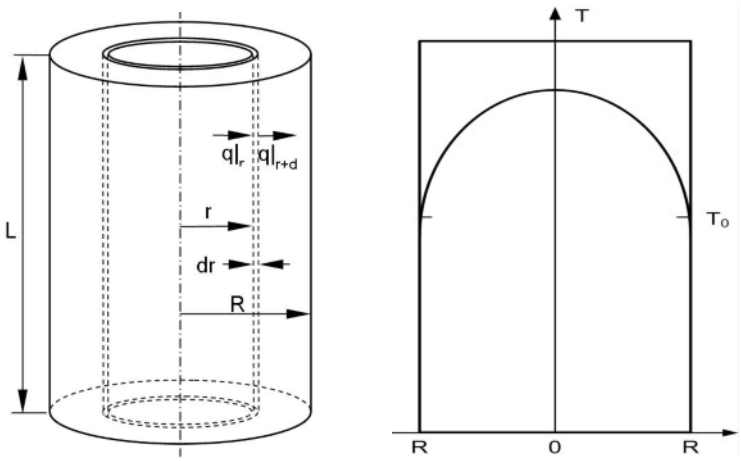

(a) (b)

Figure 5.36. Cylinder model for temperature calculation [12]: (a) a cylinder model (b) temperature distribution

$$(2\pi r dr L)\dot{q} + 2\pi r L q\big|_r = 2\pi(r+dr)Lq\big|_{r+dr} \tag{5.16}$$

where $\dot{q}$ is the rate of heat production per unit volume. For resistant heating methods, $\dot{q}$ is given by

$$\dot{q} = \frac{I^2}{k_e} \tag{5.17}$$

where k_e is the electric conductivity and I is the electric current.

Here $\dot{q}$ can be treated as a constant; then the following expression can be obtained:

$$\frac{d}{dr}(rq) = \dot{q}\, r \tag{5.18}$$

Using the Fourier law of heat transfer:

$$q = -\alpha \frac{dT}{dr} \tag{5.19}$$

where α is the thermal conductivity.

By substituting Equation (5.19) into Equation (5.18) the following expression can be obtained:

$$\frac{d}{dr}\left(r\frac{dT}{dr}\right) = -\frac{\dot{q}\, r}{\alpha} \tag{5.20}$$

$$\frac{dT}{dr} = -\frac{\dot{q}\, r}{2\alpha} + \frac{C_1}{r} \tag{5.21}$$

After further integration this gives

$$T = -\frac{\dot{q}\, r^2}{4\alpha} + C_1 \ln r + C_2 \tag{5.22}$$

Because the flux of heat production is equal to the flux of heat dissipation at the surface, the associated boundary conditions can be written as

$$\dot{q}\,\pi R^2 L = -2\pi\alpha R L \frac{dT}{dr}\Big|_{r=R} \tag{5.23}$$

$$r=R,\ T=T_0 \tag{5.24}$$

Equation (5.23) becomes

$$\frac{dT}{dr}\Big|_{r=R} = -\frac{\dot{q}R}{2\alpha} \tag{5.25}$$

By comparing Equation (5.20) with Equation (5.25), $C_1=0$. According to other boundary conditions, $T=T_0$ at $r=R$, the integral constant of C_2 is found to be

$$C_2 = T_0 + \frac{\dot{q}R^2}{4\alpha} \tag{5.26}$$

Hence, Equation (5.22) becomes

$$T = T_0 + \frac{\dot{q}R^2}{4\alpha}[1-(\frac{r}{R})^2] \tag{5.27}$$

Equation (5.28) expresses the relationship between temperature (T) and position (r) along the radial direction of the preform. It is a parabolic profile from the central axis of the cylinder, as shown in Figure 5.36b.

5.5 Liquid-immersion Chemical Vapour Infiltration

5.5.1 General Description

The discussion in Section 5.4 clearly indicates that a temperature gradient has a significant influence on the densification of the preform. In order to increase the densification rate and improve the density, it is necessary to establish a very steep thermal gradient within the preform. In 1984 Houdayer *et al.* [52] described a method for rapid densification by immersing the preform into a liquid precursor at high temperatures to fabricate the C/C composites. This densification process is also called liquid-immersion CVI (LI-CVI).

As shown in Figure 5.37 the preform is placed on a graphite mandrel, which is immersed in a liquid precursor. The mandrel is located at the lower part of the reactor, which has an opening through which a shaft is connected to a motor. The motor outside the reactor in turn rotates the graphite mandrel in the liquid precursor. The graphite mandrel is also used as a heating element coupled with the electromagnetic field from the induction coils. The infiltration temperature generated is in the range 1000 to 1300°C, which is sufficiently high to cause the liquid precursor to be vaporised. The vaporised precursor gases penetrate into the perform and then pyrolysed to form pyrocarbon deposited on the fibre surface.

There are two outlet ports located at the upper position of the reactor. One is used to introduce the liquid precursor and the other to introduce inert gas for expelling the air contained inside before the infiltration process commences. At the top of the reactor there is a water-cooling condenser to separate the unconsumed vaporised liquid precursor from exhaust gases.

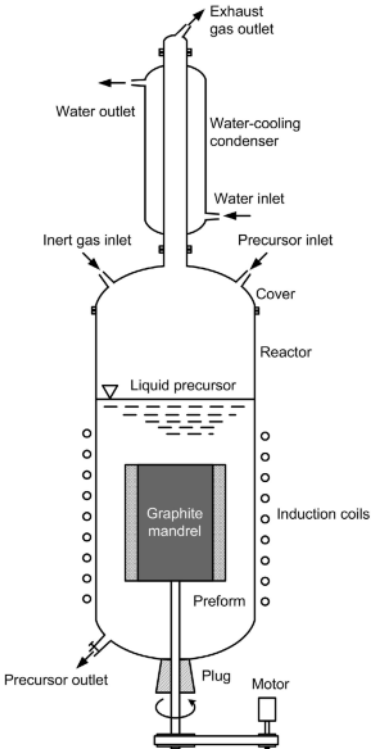

Figure 5.37. Illustration of liquid-immersion CVI reactor [52]

In this technique cyclohexane (C_6H_{12}) is selected as a liquid precursor because of its suitable boiling point, low toxicity and low cost. In addition, some other hydrocarbons also exhibit infiltration properties similar to those of cyclohexane,

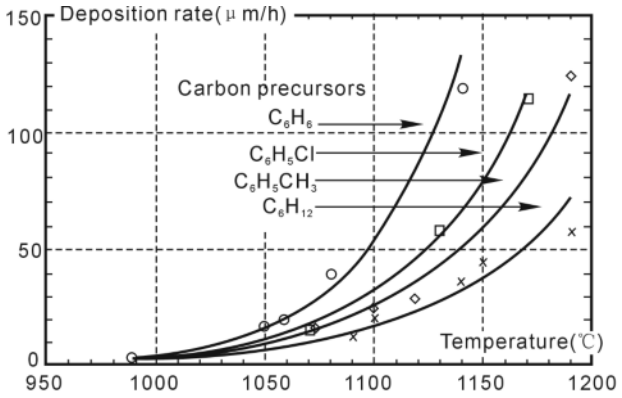

Figure 5.38. Deposition rate comparison of several carbon precursors [42]

Table 5.1. Some commonly used precursors and the corresponding materials deposited [10]

Deposit	Liquid precursor
C	C_5H_{10}, C_6H_{12}, C_6H_6, $C_6H_5CH_3$ and C_6H_5Cl, gasoline, etc.
BN	Trichlorobozaine ($B_3N_3Cl_3H_3$), borazine (B_3NH_6)
SiC	Methyltrichlorosilane CH_3SiCl_3, dimethyldichlorosilane $(CH_3)_2SiCl_2$, and methyldichlorosilane $((CH_3)_2SiHCl_2$
SiC–Si_3N_4	Tris-n-methyl-amino-silane, silazane
SiO_2	$Si(OC_2H_5)_4$

including $C_6H_5CH_3$, C_6H_6 and C_6H_5Cl. As illustrated in Figure 5.38, both aromaticity and the presence of halogen in the above precursors increase the conversion efficiency and the yield. Some commonly used precursors for other deposit materials are listed in Table 5.1.

For the liquid-immersion CVI process a very steep thermal gradient is established within the preform at the initial infiltration, ranging from 400 to 500°C·min^{-1}. This then decreases because the parts successively densified reach a temperature closer to that of the heating element. As the temperature is increased from 900 to 1200°C, the densification rate is significantly increased from 0.02 g·min^{-1} to 1.25 g·min^{-1}, as listed in Table 5.2. However, undesirable deposition behaviour occurs if the temperature is further increased; the preforms become less dense in the inner region than in the outer region. In such cases, regions far from the susceptor reach a temperature higher than that of hydrocarbon pyrolysis, thus leading to densification at the outer regions or extremes of the preform before the intermediate regions are completely infiltrated.

5.5.2 Model of Liquid-immersion Chemical Vapour Infiltration

Based on experimental results an overall model of the LI-CVI process is proposed by Rovillain [42], as shown in Figure 5.39. Starting from the centre of the heating element the reactor is divided into five zones, each of them characterised by a specific function.

Zone I: Heating Resource

The first zone is characterised by its function of generating sufficient heat for the CVI process. This heating source is also required to maintain a constant temperature (T) during the CVI process. The heating source initially includes only

Table 5.2. Relationship between densification rate and processing temperature [53]

Temperature (°C)	900	1000	1050	1100	1200
Densification rate (g·min^{-1})	0.02	0.10	0.25	0.45	1.25

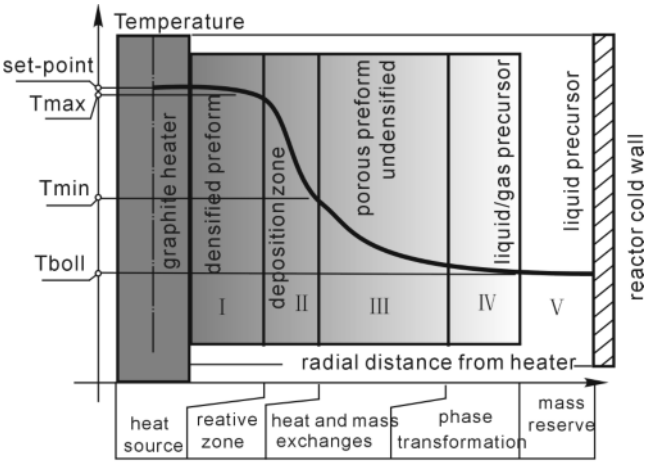

Figure 5.39. LI-CVI process model of [42]

the graphite heater, but as the preform is gradually densified and becomes C/C composites this also become a part of the heating source. The heat is transferred outwards by a thermal conductive mechanism to the adjacent zones. Within this zone the temperature gradient is very small.

Zone II: Reactive Zone

The reactive zone is the region where chemical vapour infiltration takes place through many complex chemical reactions. The reactive zone is narrow. There is a very steep thermal gradient within this zone to facilitate the infiltration process. In Figure 5.39 T_{max} and T_{min} are the maximum temperature and minimum temperature for deposition respectively.

The pyrolysis of the precursors is a complex process and it produces a large number of intermediate species. The composition of the exhaust gases can be analysed by gas phase chromatography. The by-products listed in Table 5.3 are generally the same within temperature range of 1000 to 1350°C when cyclohexane

Table 5.3. Exhaust gas analysis results by GPC (mol%) [53]

T(°C)	H_2	CH_4	C_2H_2	C_2H_4	C_2H_6	C3	C4	C_6H_{12}
1000	21.1	11.6	0.5	31.1	5.2	6.9	18.1	5.5
1100	36.2	12.8	2.5	27.7	1.0	4.5	ND	7.5
1250	49.1	13.3	4.5	16.5	0.4	1.2	ND	ND
1350	45.3	13.1	4.0	21.4	0.6	1.7	ND	ND

Note: (1) C_6H_{12} is used as the liquid precursor; (2) C3 and C4: undetermined C3 and C4, species; (3) ND: non-detected products.

is utilised as the liquid precursor. However, their relative proportions depend on the processing temperature. The amount of hydrogen and the lightest hydrocarbons (mainly methane and ethylene) is increased as the temperature increases. By contrast, the proportion of the heaviest gaseous compounds, especially C3 and C4 species and cyclohexane, becomes less and less important as the processing temperature is increased above 1250°C. These studies clearly reveal that, as expected, cyclohexane is firstly vaporised and then decomposed in a great number of compounds.

Zone III: Heat and Mass Exchange Zone

This is the area within the porous preform where the complex heat and mass exchanges occur. In this multiphase system the heat is transferred outwards through convective and radiation mechanisms. The precursor gases are supplied from the outside towards the reactive zone while the exhaust gases are transferred in the reverse direction after the chemical reactions.

Zone IV: Phase Transformation Zone

The liquid precursor is transformed into gaseous reactants and the function of this zone is to ensure a sufficient liquid-to-gas-phase transformation. The liquid precursor is vaporised on the outer surface of the preform where the temperature is maintained just above the boiling point of the liquid precursor. In this case the boiling point refers to the temperature at atmospheric pressure for a given hydrocarbon.

Zone V: Mass Reserve Zone

The outside zone is used to store the reserve liquid precursor in a mass reservoir, which surrounds the preform in a fully immersed manner. Outside of the preform the liquid forms a 'turbulent' boiling fluid with many bubbles due to cavitation and the outgoing gases. The cavitation phenomenon is a two-phase process in which bubbles or voids in the heated liquid precursor are formed.

The in-depth model of the deposition process is another important aspect of gaining a deep understanding of an LI-CVI process as well as a TG-CVI process. Under a strong thermal gradient the relationship between the deposition rate on a fibre (u_{dep}) and the densification rate inside the preform (u_{front}) can be calculated by using the one-dimensional model [42].

As shown in Figure 5.40, the regularly arranged fibres are perpendicular to the reaction front. The spacing between fibres is d and the deposition location along the fibre is f. Based on experimental observation both u_{dep} and u_{front} can be expressed as

$$u_{dep} = k \exp(-\frac{E_a}{RT}) \tag{5.29}$$

$$u_{front} = \frac{df}{dt} \tag{5.30}$$

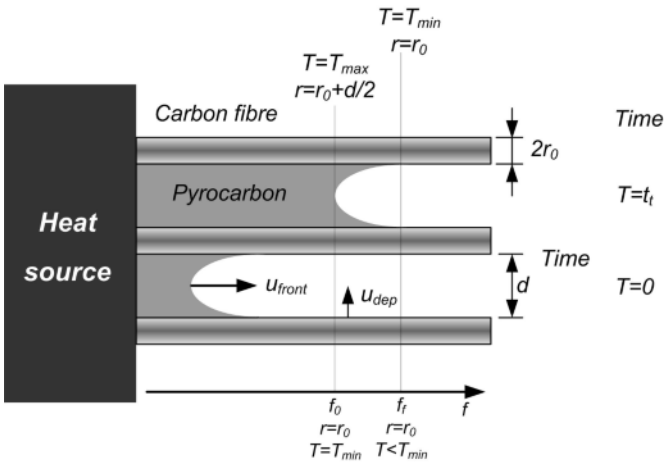

Figure 5.40. One-dimensional model for LI-CVI process [42]

As the deposition advances the fibre becomes thicker and thicker. The radius of the coated fibre is then expressed as

$$r = r_0 + \int_0^t u_{dep} dt = r_0 + \int_{f_0}^{f_f} u_{dep} \frac{df}{u_{front}} \tag{5.31}$$

At t_f the coated fibre radius is $r = r_0+d/2$, and the front location is f_f. Then we can obtain

$$u_{front} = \frac{2}{d} \int_{f_0}^{f_f} u_{dep} df \tag{5.32}$$

Considering that the temperature gradient is constant in the thickness of the densification front the precursor starts to be pyrolysed between the deposition temperature T_{max} and the lowest temperature T_{min}. Then the front densification rate is the function of T_{max} and temperature gradient ∇T. This is expressed as

$$u_{front} = \frac{2}{d} \int_{T_{min}}^{T_{max}} u_{dep} \frac{df}{dT} dT = \frac{2k}{d|\nabla T|} \int_{T_{min}}^{T_{max}} \exp(-\frac{E_a}{RT}) dT \tag{5.33}$$

where R is the perfect gas constant, k is the chemical reaction constant and E is the active energy of the chemical reaction.

5.6 Pulsed Chemical Vapour Infiltration

5.6.1 General Description

For most reactions in CVD processes the volume of the by-products is larger than those of the reactant gases, as exemplified by Equation (5.1); therefore, fresh reactant gases have to penetrate through the outgoing stream of by-product gases in order to reach new areas, at deeper locations, for further deposition. This is the main cause of the long densification time and relatively high residual porosity.

Based on pulsed CVD (P-CVD) by Bryant [55] in 1976 Sugiyama [56, 57] proposed the pulsed CVI method (P-CVI). The aim is to accelerate the in-diffusion of fresh precursor species and the out-diffusion of the by-products to and from the pores of the preform and thereby reduce the total infiltration time and density gradient along the thickness of the composites. The instantaneous introduction of precursor gases ensures the uniformity of the precursor gas composition along the depth of the pores within the preform and leads to uniform dense composites.

The typical system architecture for a P-CVI process is shown in Figure 5.41. For silicon carbide infiltration hydrogen gas after a purification process is mixed with argon and then bubbled through a CH_3SiCl_3 liquid precursor. The precursor gases are then accumulated in a reservoir from which the gases are fed into the reaction chamber instantaneously during the gaseous reactant injection phase of the P-CVI cycle. This is controlled by the electromagnetic valve at a preset pressure. Then, the inlet electromagnetic valve is closed for the second phase of the cycle, deposition, and the gases are kept in the chamber for a given time to allow the SiC deposition process to occur. Finally the outlet electromagnetic valve is opened to evacuate the deposition chamber and all by-products are purged for a new cycle. This is the last phase of the cycle evacuation. The total volume of the pipes, dead spaces and reaction chamber is minimised to satisfy the requirements of high gas yield and short evacuation time.

The above three-phase (namely gaseous reactant injection, deposition and evacuation) cycle is repeated for the whole duration of the P-CVI process until a product is finished. The inlet and outlet valves opening and closing are typically controlled with a computer system.

5.6.2 Model

As described above P-CVI works on the principle of alternative injection of reactant gases, deposition and evacuation of CVI exhaust gases. This is required to rapidly transport reactant species into, and by-product gases out of, the preform at isothermal conditions. For each cycle the detailed sequence generally consists of the following essential and sequential steps, as shown in Figure 5.42:

1. rapidly injecting the precursor into the fully evacuated CVI chamber at a predetermined pressure,
2. holding the precursor gases for a preset period (also known as duty cycle) during which deposition occurs under a designed condition at a preset pressure and temperature, and

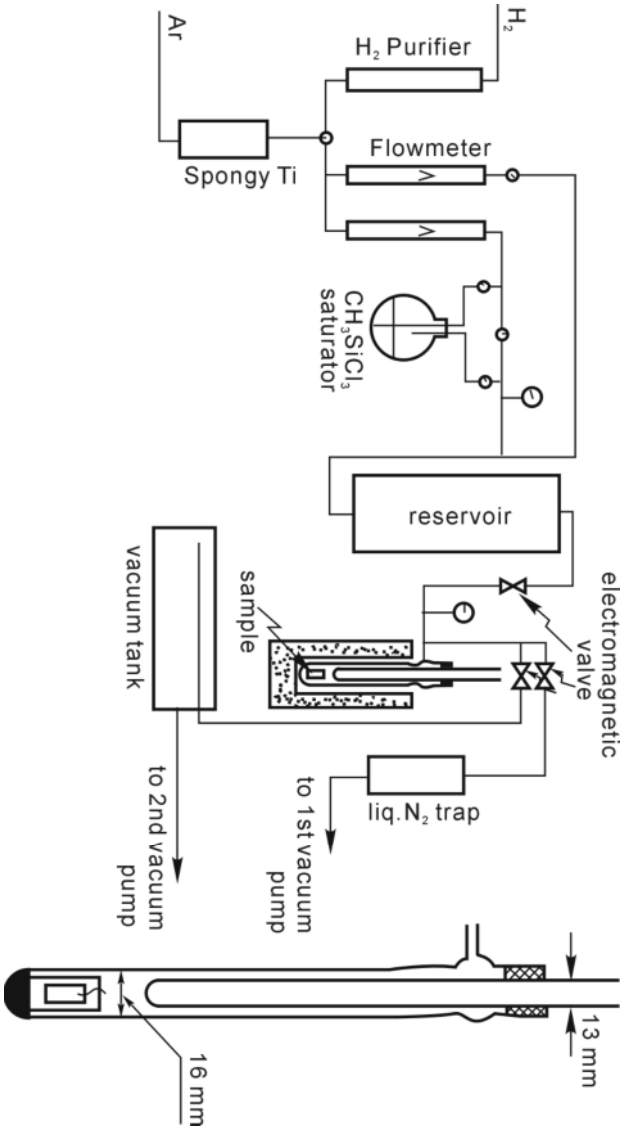

Figure 5.41. Apparatus for pulsed CVI of SiC [57]

3. rapidly evacuating the by-product gases from the reaction chamber.

Depending on the requirement of the vacuum level generated during the evacuation phase sometimes it is necessary to introduce a period of time in the cycle to purge the exhaust gases further to ensure a thorough evacuation. During this process the inlet valve is fully closed and the outlet valve is kept open.

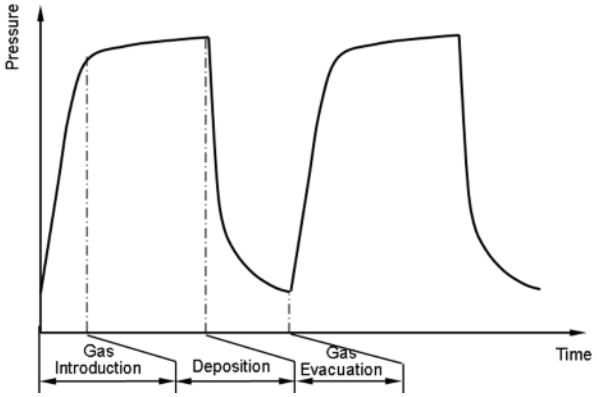

Figure 5.42. Elementary sequences for a P-CVI process

At each cycle or pulse the reactor is first evacuated at a reduced level pressure, 0.05 to 0.1 kPa, at the end of the previous cycle. The precursor gases are injected into the reactor within a pressure range of 1~10 kPa within a few seconds. Then the reactor is sealed off for infiltration for a period of holding time (t_h), which can be easily controlled in a wide range, typically from 0.2 to 120 s. Each pulse ends with the evacuation stage which takes a few seconds. These steps are repeated many times.

The P-CVI processing parameters include the deposition temperature and pressure, precursor injection time, holding time, evacuation time and the number of pulses.

The overall model of a P-CVI process is as shown in Figure 5.43. During a P-CVI process the mass transport of gaseous species can be divided into two stages. In the first stage mass transport takes place by forced convection within a very short period of a few hundredths or tenths of a second. In the second stage of the duty cycle the mass transport is dominated by the diffusion from the free space of the reaction chamber into the pores of the fibre preform. The temperature is kept

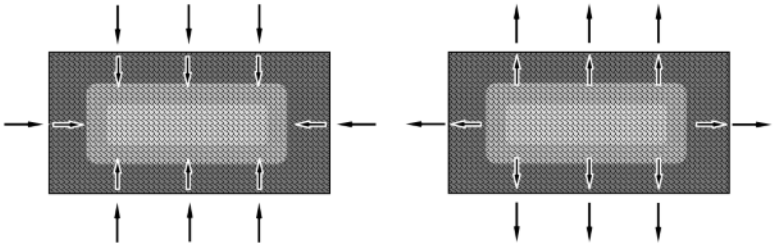

Figure 5.43. Overall model of a P-CVI process: (a) during gas introduction and (b) during gas evacuation

constant throughout the whole process. Accordingly, this process can be considered another form of I-CVI process operated within a very short time and regularly interrupted by a number of pulses. In other words, P-CVI is transformed into I-CVI if the duty cycle is increased from a few seconds to a few hours.

5.6.3 Applications

At the initial development period of the P-CVI process it was considered a novel way to increase the densification rate and to minimise the density gradient of the composites. However, this technique is difficult to scaleup because it is very difficult, or impossible, to evacuate a large reaction chamber within a very short time. In spite of that, this approach provides some useful information to understand the infiltration mechanisms and to tailor the materials according to the requirements [58]. For example, the residence time of the reactant gases in a P-CVI process can be accurately controlled. Hence, it is helpful to understand the influence of homogeneous reactions and evolution of the reactant gases on the microstructure characteristics of the deposit. Furthermore, multilayered materials can be fabricated if different precursors are alternately introduced into the reaction chamber. Multilayered deposits of $(PyC\text{-}SiC)_n$ are prepared in this way; pyrocarbon (PyC) and silicon carbide (SiC) are deposited from hydrocarbon gas (C_xH_y) and methyltrichlorosilane (MTS-H_2) respectively. The thickness of the sublayer can be elaborately fabricated in a large-scale range by controlling the processing parameters of temperature, pressure and holding time.

One of the distinct applications of the P-CVI technique is fabricating highly engineered composites with a multilayered interphase and matrix, which exhibit self-healing behaviour in an oxidising environment. Figure 5.44a shows the microstructure of a composite which has a self-healing matrix consisting of four sequences–S1, S2, S3 and S4. Each sequence includes four sublayers of $C(B)/B_{13}C_2/C(B)/SiC$. Both S1 and S2 are located in the inner region and have a very thin thickness of 1 μm. By contrast, the S3 and S4 sequences are located in the outer region and their thicknesses are 4 μm and 6 μm respectively. It is interesting to note that the multistep pull-out of the fibre from the matrix is observed from the fracture surface as shown in Figure 5.44b and c.

The boron-doped pyrocarbon sublayer of C(B) is used as the mechanical fuse which ensures crack deflection and fibre pull-out. A hydrocarbon (C_xH_y) and BX_n(X=F or Cl) are used as reactant precursors to deposit the C(B) layer. Both $B_{13}C_2$ and SiC are employed as the glass former to improve the oxidation resistance of the composite. $B_{13}C_2$ is deposited with the same precursors as for C(B) but in different conditions. CH_3SiCl_3 and H_2 are used as the precursor gases for the SiC deposition.

Figure 5.45 shows examples of the self-sealing behaviour of this composite. The B_2O_3–SiO_2 glass is formed at high temperature after boron carbide ($B_{13}C_2$) and silicon carbide (SiC) are oxidised in the oxidising atmosphere. The glass has sufficient fluidity and can fill the microcracks and defects within the composite. The incoming oxygen is consumed by *in-situ* reactions with boron carbide and silicon carbide such that the oxygen transport access is efficiently blocked off by

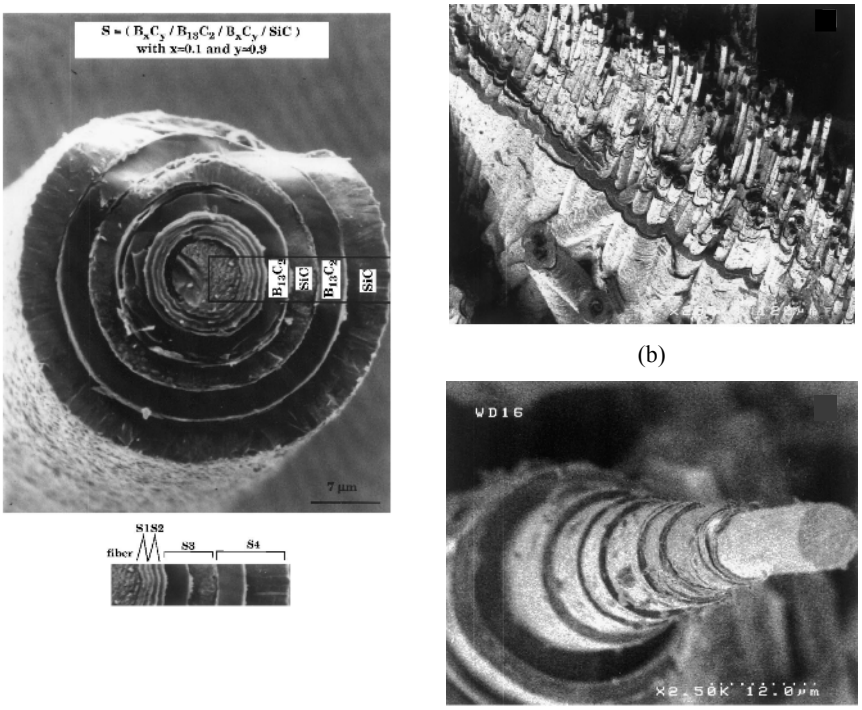

(a) (b) (c)

Figure 5.44. SEM graphs of multilayered matrix composite by P-CVI: (a) details of four sequences on a single fibre [23], (b) fracture surface of 2.5-D C/SiC composite [59], (c) fracture surface of a single fibre [59]

B_2O_3–SiO_2 glass. Hence, the oxidation resistance of the composite is greatly improved by the multilayered matrix.

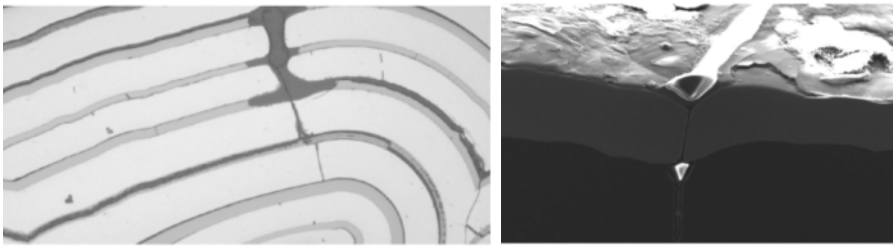

(a) (b)

Figure 5.45. Self-sealing composites [33]: (a) self-sealing sequences and (b) glass-filled cracks

5.7 Chemical Vapour Composite

The chemical vapour composite (CVC) process was developed by ThermoTrex Corporation [60, 61] to fabricate materials by simply mixing reinforcement elements such as particles, whiskers and fibres with precursor gases, which are then transported and co-deposited on a substrate. A schematic of a CVC SiC reactor is shown in Figure 5.46. One distinct advantage of this technique is flexibility in controlling the variation of density, geometry and composition of the reinforcement during deposition. The process can fabricate composite components to the net shape (±0.013 mm) on a machined substrate in a single run.

The advantages of the CVC process are as follows: fast growth rate of the composites (about 100 times faster than conventional techniques because the precursor gases need not infiltrate into a preform), no need for expensive fibre performs, possible to use high modulus fibres in the composites and high accuracy of deposited composites without further machining. However, the CVC technique also suffers the weakness of having a low fibre volume fraction in the composites and using only short fibre, resulting in inferior mechanical properties of the composites.

During CVC processing, a CH_3SiCl_3 precursor is bubbled and delivered by the H_2 carrier gas. Then the reactant gases and reinforcements are mixed together and injected onto the graphite substrate, which is heated at a preset temperature. Like a CVD process, a CVC process can essentially produce a uniform layer of deposit onto the surface of the substrate. Hence, it allows the geometry of the base

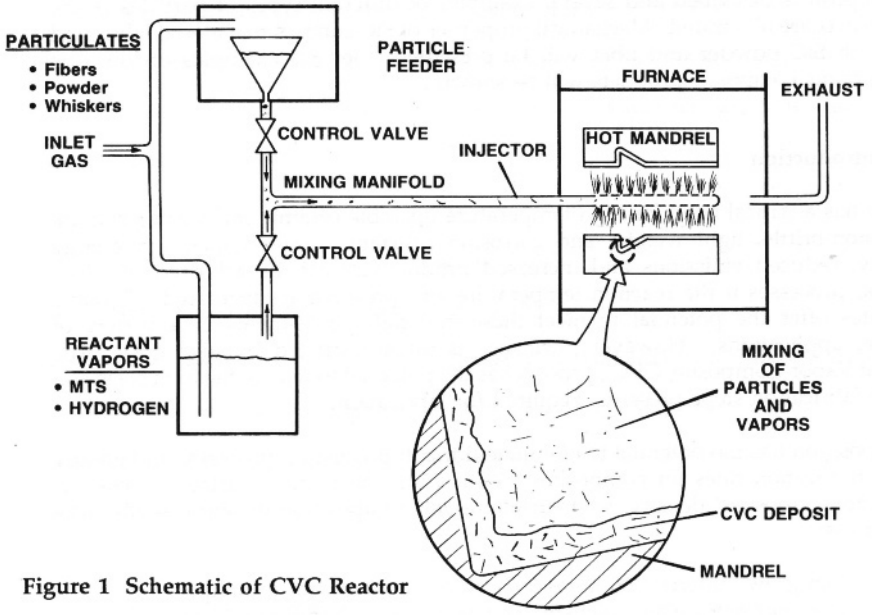

Figure 5.46. Schematic of CVC SiC reactor [60]

(a)

(b)

Figure 5.47. Microstructure of C/SiC (a) and some components (b) by the CVC technique [60]

component substrate to be replicated. Figure 5.47a shows the microstructure of the components fabricated by the CVC technique. Figure 5.47b shows some typical examples of the components produced by using the CVC technique. It can be seen that components in a range of complex shapes have been manufactured.

References

[1] Bickerdike RL, Brown ARG, Hughes G, Ranson H (1962) In: Mrosowski S, Studebaker MC, Walker PL (eds) Proceedings of 5th conference on carbon, vol 1. Pergamon, New York, p575

[2] Jenkins WC (1964) Method of depositing metals and metallic compounds throughout the pores of a porous body. US Patent 3,160,517

[3] Kotlensky WV (1973) Deposition of pyrolytic carbon in porous solid. In: Walker PL Jr, Thrower PA (eds) Chemistry and physics of carbon. Dekker, New York, vol 9, pp173–262:

[4] Fitzer E, Hegen D, Strohmeier H (1979) Chemical vapor deposition of silicon carbide and silicon nitride and its application for preparation of improved silicon ceramics. In: Sedgwick TO, Lydtin H (eds) Proceedings of the 7th international conference on chemical vapour deposition. Electrochemical Society, Pennington, NJ, pp525–535
[5] Christin F, Naslain R, Bernard C (1979) A thermodynamic and experimental approach of silicon carbide CVD. Application to the CVD-infiltration of porous carbon composites. In: Sedgwick TO, Lydtin H (eds) Proceedings of the 7th international conference on chemical vapour deposition. Electrochemical Society, Pennington, NJ, pp499–514
[6] Caputo AJ, Lackey WJ (1984) Fabrication of fibre-reinforced ceramic composites by chemical vapor infiltration. Ceram Eng Sci Proc 5:654–667
[7] Fitzer E, Fritz W, Schoch G (1991) The chemical vapor impregnation of porous solids, modeling of the CVI-process. J de Physique IV 2:C-2-143–150
[8] Naslain R (1992) CVI composites. In: Warren R (ed) Ceramic-matrix composites. Chapman & Hall, New York, pp199–244
[9] Besmann TM, Sheldon BW, Lowden RA, Stinton DP (1991) Vapor-phase fabrication and properties of continuous-filament ceramic composites. Science 253:1104–1109
[10] Golecki I (1997) Rapid vapor-phase densification of refractory composites. Mater Sci Eng R20:37–124
[11] Christin F (2002) Design, fabrication and application of thermostructural composites (TSC) like C/C, C/SiC, and SiC/SiC composites. Adv Eng Mater 4:903–912
[12] Bird RB, Stewart WE, Lightfoot EN (1960) Transport Phenomena. Wiley, New York
[13] Kalidindi SR, Desu SB (1990) Analytical model for the low pressure chemical vapor deposition of SiO_2 from tetraethoxysilane. J Electrochem Soc137:624–628
[14] Starr TL (1992) Advance in modeling of the chemical vapor infiltration process. In: Besmann TM, Gallois BM, Warren JW (eds) Chemical vapor deposition of refractory metals and ceramics II. Materials Research Society, Pittsburgh, PA, pp207–214
[15] Thomas JM, Thomas WJ (1997) Principles and practice of heterogeneous catalysis, VCH, Weinheim
[16] Fedou R, Langlais F, Naslain R (1990) On the modeling of the chemical vapor infiltration of SiC-based ceramics in a straight cylindrical pore. In: Spear KE, Cullen GW (eds) Proceedings of the 11th international conference on chemical vapour deposition. Electrochemical Society, Pennington, NJ, pp513–524
[17] Marinkovic S, Dimitrijevic S (1985) Carbon/carbon composites prepared by chemical vapour deposition. Carbon 23:691–699
[18] Clegg WJ, Kendall KMN, Alford N, Button TW, Brichall JD (1990) A simple way to make tough ceramics. Nature 347:455–457
[19] Evans AG (1990) Perspective on the development of high-toughness ceramics. J Am Ceram Soc 73:187–206
[20] Dugne RO, Guette A (1991) Boron nitride interphase in ceramic-matrix composites. J Am Ceram Soc 74:2482–2488
[21] Tressler RE (1999) Recent developments in fibres and interphases for high temperature ceramic matrix composites. Composites A30:429–437
[22] Brennan JJ (1990) Interfacial studies of chemical-vapour-infiltrated ceramic matrix composites. Mater Sci Eng A126: 203–223
[23] Naslain R, Pailler R, Bourrat X, Bertrand S, Heurtevent F, Dupel P, Lamouroux F (2001) Synthesis of highly tailored ceramic matrix composites by pressure-pulsed CVI. Solid State Ion 141-142:541–548

[24] Xu YD, Cheng LF, Zhang LT, Yin HF, Yin XW (2001) Mechanical properties of 3D fibre reinforced C/SiC composites. Mater Sci Eng A300:196–202
[25] Lamouroux F, Bourrat X, Naslain R (1993) Structure/oxidation behavior relationship in the carbonaceous constituents of 2D-C/PyC/SiC composites. Carbon 31:1273–1288
[26] Lackey J, Hanigofsky JA, Freeman GB, Hardin RD, Prasad A (1995) Continuous fabrication of silicon carbide fibre tows by chemical vapor deposition. J Am Ceram Soc 78:1564–1570
[27] Ochiai S, Hojo M, Tanaka M (1999) Mechanical interactions between fibre and cracked coating layer and their influences on fibre strength. Composites A30:451–461
[28] Naslain R, Lamon J, Pailler R, Bourrat X, Guette A and Langlais F (1999) Micro/minicomposites: a useful approach to the design and development of non-oxide CMCs. Composites A30:537–547
[29] Morgen P (2005) Carbon fibres and their composites. Taylor & Francis, London, p565
[30] Bouquet C, Fischer R, Thebault J, Soyris P, Uhrig G (2005) Composite technologies development status for scramjet. In: Proceedings of AIAA/CIRA 13th International Space Planes and Hypersonics Systems and Technologies :AIAA-2005-3431, Capua, Italy
[31] Ohnabe H, Masaki S, Onozuka M, Miyahara K, Sasa T (1999) Potential application of ceramic matrix composites to aero-engine components. Composites A30:429–437
[32] Naslain R, Christin F (2003) SiC-matrix composite materials for advanced jet engines. MRS Bull:28:9:654–658
[33] Christin FA (2005) A global approach to fibre nD architectures and self-sealing matrices: from research to production. Int J Appl Ceram Technol 2:97–104
[34] Bouquet C, Fischer R, Larrieu JM, Uhrig G and Thebault J (2003) Composite technologies development status for scramjet applications. In: Proceedings of 12th AIAA International Space Planes and Hypersonics Systems and Technologies :AIAA-2003-6917, Norfolk, VA
[35] Caputo AJ, Lackey WJ (1984) Fabrication of fibre reinforced ceramic composites by chemical vapour infiltration. Ceram Eng Sci Proc 5:654–667
[36] Stinton DP, Lowden RA, Besmann TM (1992) Fibre-reinforced tubular composites by chemical vapour infiltration. In: Besmann TM, Gallois BM, Warren JW (eds) Chemical vapour deposition of refractory metals and ceramics II. Materials Research Society, Pittsburgh, PA, pp233–238
[37] Besmann TM, McLauglin JC, Lin HT (1995) Fabrication of ceramic composites: forced CVI. J Nucl Mater 219:31–35
[38] Vaidyaraman S, Lackey WJ, Freeman GB, Agrawal PK, Langman MD (1995) Fabrication of carbon-carbon composites by forced flow-thermal gradient chemical vapour infiltration. J Mater Res 10:1469–1477
[39] Tsai CY, Desu SB (1992) Contribution of gas-phase reactions to the deposition of SiC by a forced-flow chemical vapor infiltration process. In: Besmann TM, Gallois BM, Warren JW (eds) Chemical vapour deposition of refractory metals and ceramics II. Materials Research Society, Pittsburgh, PA, pp227–232
[40] Snead LL, Jones RH, Kohyama A, Fenici P (1996) Statue of silicon carbide composites for fusion. J Nucl Mater 233-237:26–36
[41] Gupte SM, Tsamopoulos JA (1989) Densification of porous materials by chemical vapor infiltration. J Electrochem Soc 136:555–561
[42] Rovillain D, Trinquecoste M, Bruneton E, Derre A, David P, Delhaes P (2001) Film boiling chemical vapor infiltration: an experimental study on carbon/carbon composites materials. Carbon 39:1355–1365

[43] Buckley JD (1988) Carbon-carbon: a overview. Am Ceram Soc Bull 67:364–368
[44] Stoller HM, Frye ER (1972) SAMPE. Q3:10–12
[45] Lieberman ML, Curlee RM, Brannten FH, Noles GT (1975) CVD/PAN preform carbon/carbon composites. J Comp Mater 9:337–346
[46] Golecki I, Morris RC, Narasimhan D (1994) Method of rapid densifying a porous structure. US Patent 5,348,774
[47] Golecki I (2003) Industrial carbon chemical vapor infiltration (CVI) processes. In: Delhaes P (ed) Fibre and composites. Taylor & Francis, London, pp112–138
[48] Zhao JG, Li KZ, Li HJ, Wang C (2006) The influence of thermal gradient on pyrocarbon deposition in carbon/carbon composites during the CVI process. Carbon 44:786–791
[49] Tang ZH, Qu DN, Xiong J, Zou ZQ (2003) Effect of infiltration conditions on the densification behavior of carbon/carbon composites prepared by a directional-flow thermal gradient CVI process. Carbon 41:2703–2710
[50] Tang SF, Deng JY, Wang SJ, Liu WC (2007) Fabrication and characterization of C/SiC composites with large thickness, high density and near-stoichiometric matrix by heaterless chemical vapor infiltration. Mater Sci Eng A465:290–294
[51] Tang SF, Deng JJ, Du HF, Liu WC, Yang K (2005) Fabrication and microstructure of C/SiC composites using a novel heaterless chemical vapor infiltration technique. J Am Ceram Soc 88:3253–3255
[52] Houdayer M, Spitz J, Tran-Van D (1984) Process for the densification of a porous structure. US Patent 4,472,454.
[53] Bruneton E, Narcy B, Oberlin A (1997) Carbon-carbon composites prepared by a rapid densification process I: Synthesis and physico-chemical data. Carbon 35:1593–1598
[54] Vignoles GL, Goyheneche JM, Sebastian P, Puiggali JR, Lines JF, Lachaud J, Delhaes P, Trinquecoste M (2006) The film-boiling densification process for C/C composite fabrication: from local scale to overall optimization. Chem Eng Sci 61:5636–5653
[55] Bryant WA (1976) Producing extended area deposits of uniform thickness by a new chemical vapour deposition technique. J Cryst Growth 35:257–261
[56] Sugiyama K, Nakamura T (1987) Pulse CVI of porous carbon. J Mater Sci Lett 6:331–333
[57] Sugiyama K, Yamamoto E (1989) Reinforcement and antioxidizing of porous carbon by pulse CVI of SiC. J Mater Sci 24:3756–3762
[58] Dupel P, Bourrat X, Pailler R (1995) Stucture of pyrocarbon infiltration by pulse-CVI. Carbon 33:1193–1204
[59] Lamouroux F, Bertrand S, Pailler R, Naslain R, Cataldi M (1999) Oxidation-resistant carbon-fibre-reinforced ceramic-matrix composites. Composites Sci Technol 59:1073–1085
[60] Reagan P (1993) Chemical vapor composites (CVC). J de Physique IV 2:C3-541–548
[61] Reagan P, Scoville AN, Leaf R (1992) Method of forming composite articles from CVD gas streams and solid particles of fibre. US Patent 5,154,862